USING DCIN AND DCAPE TO EVALUATE SEVERE SURFACE WINDS IN THE CASE OF ELEVATED CONVECTION

A Thesis Presented to the Faculty of the Graduate School at the University of Missouri

In Partial Fulfillment of the Requirements for the Degree

Master of Science

by

PAULA SUMRALL

Dr. Patrick Market, Thesis Advisor

December 2020

The undersigned, appointed by the Dean of the Graduate School, have examined the thesis entitled

AN EVALUATION OF SEVERE SURFACE WINDS USING DCIN AND DCAPE

presented by Paula Sumrall, a candidate for the degree of master of science, and hereby certify that, in their opinion, it is worthy of acceptance.

_____

Professor Patrick Market

_____

Professor Anthony Lupo

_____

Professor Mark Palmer

_____

Professor Scott Rochette

ACKNOWLEDGEMENTS

I would like to start by thanking my advisor and committee chair, Dr. Patrick Market. He has been instrumental in my development as a student and meteorologist. In addition, I would like to thank my other committee members, Dr. Anthony Lupo, Dr Scott Rochette and Dr. Mark Palmer for being on my committee and offering valuable insights and critiques. I would like to acknowledge the University of Missouri-Columbia as well as COMET (NOAA NA16NWS4670042) for funding and for making this research possible. I would also like to thank Jason Schaumann (National Weather Service, Springfield, MO) and Greg Mann (National Weather Service, Pontiac, MI) for their contributions to some of the cases I worked on. I also would like to thank my family and friends and fellow students for their support throughout my graduate years

TABLE OF CONTENTS

LIST OF FIGURES

ABSTRACT

A series of case studies were analyzed using the ratio between the downdraft convective available potential energy (DCAPE) and the downdraft convective inhibition (DCIN). The hypothesis is that with a ratio |DCIN/DCAPE| approaching zero, momentum aloft may penetrate the stable layer and reach the surface resulting in severe criteria winds. Two case studies were preformed, the first one producing the near zero value for the ratio, and the second having a value near one for the ratio. With the first case, severe winds were observed at the surface. With the second case, winds at the surface did not reach severe criteria. However, wind damage was still observed. In addition to these cases, another case study was done over the evolution of a storm. It was noted that the majority of storms analyzed started out as either hail dominant events or wind dominant events then switch to wind dominant/hail dominant. Further analysis was done to determine how the ratio between the DCAPE and DCIN changed as the storm changed. In addition to the using the DCIN/DCAPE ratio, an analysis on the presence of gravity waves were done to determine what, if any, effect they had on convection.

CHAPTER 1. INTRODUCTION

Downdraft convective available potential energy (DCAPE) can be defined as the maximum energy available to a descending parcel of air. Mathematically it is described by Gilmore and Wicker (1998) and can be represented as:

$$DCAPE = g \int_{z_{nb}}^{z_n} \frac{\theta_v(z) - \theta_v'(z)}{\theta_v(z)} dz \tag{1.1}$$

where, $\theta_v(z)$ is virtual potential temperature of the environment at height, z, and $\theta_v'(z)$ are virtual potential temperature of the downdraft parcel. Using the Doswell and Rasmussen (1994) method, z_n is the height at which the parcel begins descending and z_{nb} is the level of neutral buoyancy (Market et al. 2017). Downdraft convective inhibition (DCIN) is defined as the downward rushing parcel that becomes warmer than its environment in the near-surface stable layer (Market et al. 2017). Mathematically DCIN can be expressed as:

$$DCIN = g \int_{z_{sfc}}^{z_{nb}} \frac{\theta_v(z) - \theta_v'(z)}{\theta_v(z)} dz \tag{1.2}$$

where, $\theta_v(z)$ is virtual potential temperature of the environment at height, z, and $\theta_v'(z)$ are virtual potential temperature of the downdraft parcel with the upper bound being the level of neutral buoyancy and the lower bound being the surface.

At its origin downdraft convective available potential energy (DCAPE) and downdraft convective inhibition (DCIN) were used as a tool to determine if convection was truly elevated. One definition of elevated convection is convection that occurs above some stable layer near the surface (Colman 1990a). Elevated convective storms are also found to have seasonal and diurnal variability that include a primary maximum in April and a secondary maximum in September. There is still some debate in the case of storms that are truly elevated convection. Some believe that with elevated convection no surface based convective available potential energy (CAPE) is present (Colman 1990a), while others have found that there can be some surface based CAPE present, but elevated convection can still dominate the storm (Corfidi et al. 2008).

Understanding the lifting mechanisms is crucial in predicting an elevated convective event that could produce severe weather. To better understand the state of the environment, the CAPE is commonly assessed using the most unstable parcel. More work needs to be done to determine what type of severe weather these elevated convective events will produce.

Thunderstorms over a frontal boundary must meet the following criteria defined by Colman (1990a) follows:

1. The storm must occur on the cold side of the analyzed surface front with distinctions between temperature, dewpoint, and wind
2. Temperature, dewpoint, and wind must be similar in the areas surrounding the chosen location

3. On the warm side of the front, the surface temperature must have a higher equivalent potential temperature than the surface temperature on the cold side of the front.

In addition to these criteria Colman (1990a) also suggest that environment that these thunderstorms form in, have strong baroclinicity, large vertical wind shear and warm air advection. Elevated thunderstorms that meet the criterion listed above, were found to have convection in a layer above a significant and often times shallow frontal inversion (Grant 1995). It is this frontal inversion that represents the stable layer that the downdraft would need to penetrate to produce severe winds at the surface. The DCIN parameter can be used as a tool to measure the depth and intensity of this frontal inversion (Market et al. 2019). The DCIN parameter can be plotted as a plan view, covering a larger area than a single sounding.

It is well known that storms with elevated convection are capable of producing heavy rainfall (Rochette and Moore 1996) and snowfall (Moore et al. 1998). Elevated convective storms can also produce severe weather. A study done by Grant (1995) investigated 11 cases with 321 severe reports. From these reports, he found that 92% of the severe reports were for hail, 7% were wind and only 1% of the severe reports for tornadoes. Expanding on this work, a study was done by Horgan et al. 2007, with a larger sample to produce similar results. It was found that thunderstorms with elevated convection rarely produced only severe wind reports (Horgan et al. 2007). Further in the study by Horgan et al. (2007) it was found that while hail was forecasted rather well,

there was a lack of knowledge as to what variables produce the severe wind, making it difficult to forecast. It is in this light that the current work aims to provide a tool for forecasters to better predict when severe winds will occur at the surface.

The work with DCAPE and DCIN has evolved from a method of determining whether convection is elevated, to predicting heavy rainfall or snow, to evaluating the potential for a downdraft to penetrate a stable layer producing severe wind at the surface. In order to assess the potential for the downdraft to penetrate the stable layer, evaluating the DCAPE and DCIN together is a useful tool. DCAPE is representative of the negative buoyancy. This makes it a useful tool for determining the strength of the downdraft due to descent being related to strong negative buoyancy. When the DCIN is larger than the DCAPE the surface parcels are theoretically restricted to the sub-inversion layer this prevents parcels from becoming part of the deeper convection (Market et al. 2017). This larger DCIN makes it more difficult for the downdraft to penetrate the stable layer. For the evaluation of the potential for severe winds at the surface it is instructive to look at the DCAPE to DCIN ratio.

1.1 Objectives

Previous work by Market et al. 2019 suggests that the DCIN and DCAPE can be used to determine if the downdraft will penetrate a stable layer. This work includes an examination the ratio of |DCIN to DCAPE|. The

hypothesis is as the ratio between the DCIN and DCAPE is closer to zero, the more likely it is the downdraft will penetrate the stable layer producing severe winds at the surface. Conversely as the ratio of DCIN to DCAPE approaches 1 it is less likely for severe winds, due only to the negative buoyancy of the downdraft, to be present at the surface. In addition to this work, an analysis of the level from which the parcel was lifted is performed to determine what, if any, impact that has on the values of DCIN and DCAPE.

Another common feature that has been identified is the presence of gravity waves. All case studies in this work have some evidence of gravity wave presence. It is hypothesized these gravity waves interact with the elevated convection and have an impact on the strong winds reaching the surface.

Thus, the objectives of this research are as follows:

1. Determine to what effect the level of the parcel impacts the DCIN and DCAPE
2. Show that the DCIN to DCAPE ratio can be used as a tool to forecast severe winds at the surface
3. Determine the relationship of the DCIN to DCAPE as a storm transitions from hail dominant to wind dominant
4. Investigate the role of gravity waves and the effect on the DCIN and DCAPE

CHAPTER 2. LITERATURE REVIEW

2.1 Definitions

There has been some evolution in the research community as to what makes a thunderstorm a truly elevated event. Colman (1990a) defines elevated convection as convection that occurs above a frontal inversion where surface diabatic effects have no influence on the thunderstorm. The absence of surface diabatic effects, or no surface-based CAPE, allows for the instability to occur above a stable surface layer. Other definitions of elevated convection focus more on the stable layer and the instability above. Corfidi et al. (2008) defines elevated convection as convection where the air parcel originates from a layer above the planetary boundary layer. This occurs above a near surface stable layer, where a sloping frontal surface is present ***or*** where there is instability above the surface. It is this near-surface stable layer that will be the focus of this research.

The stable layer associated with elevated convection is an important factor in this research. The main goal of this research is to show that using the |DCIN/DCAPE| ratio can be used to determine whether a downdraft will penetrate this stable layer. Downdraft convective available potential energy (DCAPE) is defined as the maximum energy available to a descending parcel, according to parcel theory (AMS Glossary). DCAPE has commonly been used to assess the strength of the downdraft, but often falls short when forecasting for severe winds at the surface (Gilmore and Wicker 1998). Downdraft convective inhibition (DCIN) is the missing link to being able to better predict

the likelihood of a downdraft penetrating the stable layer (Market et al. 2017). DCIN can be used to measure the depth and intensity of the cold, stable sub-inversion layer (Market et al. 2019). In the past DCIN has been used to explain frontal motion and to help determine whether elevated convection will result in severe or non-severe thunderstorms (Kastman et al. 2017). This work aims to further the evolution of the DCIN parameter by using it to determine the specific type of severe threat posed by an elevated thunderstorm.

2.2 Preferred Frontal Environment for Producing Elevated Convection

Elevated thunderstorms are associated with many different types of storms including frontal systems, mesoscale convective systems, and even supercells, although these are rare. Since all types of severe weather can be produced by elevated convection, it is important to understand the environments that are favorable for producing elevated convection. The majority of elevated convective thunderstorms occur in a hydrostatically stable environment (Colman 1990a). The criteria for elevated thunderstorms as previously mentioned includes:

- the storm being located at least 50 statute miles north of a well-defined surface front.
- Temperature, wind speed and dewpoint must be similar to surrounding areas.

- On the warm side of the front the surface temperature must have a higher equivalent potential temperature than the surface temperature on the cold side of the front.

The third criteria is to ensure that the overriding air has more convective potential than the underlying boundary, ensuring the convection is elevated (Colman 1990a).

As previously mentioned, there is a bimodal seasonal pattern for elevated thunderstorms with the first peak occurring in April and the second peak occurring in September. The conditions responsible for providing the first peak of elevated convective activity in April include a cold upper atmosphere, a surface boundary layer that is becoming warmer and more moist and the southward advection of cold air from Canada that strengthens the temperature gradient. These factors allow for the environment to become more baroclinic, which is preferred in elevated convection. The second peak of elevated thunderstorms in September is due to the increased activity in extra-tropical cyclones.

In addition to a seasonal pattern discussed previously, there are also geographical and diurnal preferences in the occurrences of elevated convection. Colman (1990a) found that elevated convection tends to occur north of the central Gulf Coast along the Mississippi River Valley. He also found that nearly all storms that occur in the winter are elevated in nature and are located east of the Rocky Mountains. There is a diurnal cycle to winter events that is dependent on the type of front that contributes to the development of the

elevated thunderstorms. Storms that are associated with a warm or stationary front are more frequently found at 1200 UTC and storms associated with a cold front occur more often at 0000 UTC (Colman 1990a).

Potential instability is a good indicator of storms, both elevated and surface-based. Examining the potential instability is crucial in understanding the storm environment. The majority of severe storm report locations coincide with areas of potential instability paired with upward vertical velocities (Grant 1995). A simple way to evaluate if there is potential instability aloft is to take the difference in the values of the equivalent potential temperature (θ_e), between the 500-mb level and the 800-mb level. If the value found is negative (implying a decrease in θ_e with height), then potential instability is present. This makes the θ_e parameter important in assessing elevated convection. Warm moist air is characterized by high values of θ_e in the lower levels and this contributes to the buoyancy of the storm (Rochette and Moore 1996). This warm, moist air, with a dry layer above is responsible for creating potential instability that occurs between the layers.

It has been found that there are certain synoptic conditions that are favorable to producing elevated thunderstorms with severe threats as well as non-severe threats such as heavy rainfall or snowfall. Some features that favor heavy rainfall produced from elevated convection include a shallow thermal boundary and a low-level jet and upper-level flow pattern that aids in moisture inflow. These features produce a wind profile that suggests a slow moving and/or training echo (Market et al. 2017). Potential instability relies strongly on

high moisture availability making that a key feature in these elevated thunderstorms, especially those producing heavy rainfall. If there are potentially unstable layers in the presence of synoptic scale ascent, they become saturated and unstable. It is at this stage that vertical motions begin and could lead to heavy precipitation (Moore et al. 1998). Moisture convergence is responsible for lifting a parcel to the level of free convection, contributing to localized strong convection. This area of strong convection is typically co-located with the exit region of the low-level jet where moisture convergence is maximized (Rochette et al. 1999).

One path to creating elevated convection is the atmosphere responding to lifting that occurs above a cool, stable boundary layer ahead of a surface boundary. This lifting is a crucial factor in elevated convection, and therefore it is important to look at what factors contribute to this lifting. Large scale lift that aids in the development of potentially unstable air becoming saturated includes the strengthening of the low-level jet and a shortwave trough (Rochette et al. 1999). One approach to assessing the potential for elevated convection through lifting is to examine an isentropic surface. The equation for vertical motion on an isentropic surface is:

$$\omega_\theta = \frac{\partial p}{\partial t} + \vec{\mathrm{V}} \cdot \nabla P + \frac{d\theta}{dt}\frac{\partial P}{\partial \theta} \qquad (2.1)$$

The first right-hand-side term is local pressure tendency, while the second term is pressure advection (analogous to thermal advection on a constant pressure surface). The final term is diabatic heating/cooling rate. Warm air advection is

a large contributor to the destabilization from lifting that occurs above a frontal inversion (Grant 1995).

Another key feature in environments favorable for elevated convection is stable air below a strong frontal inversion and unstable air above (Colman 1990a). This inversion is important in elevated convection, not only because it separates stable air from unstable air, but it allows for a mid-tropospheric warming that is favored by elevated convection. The sharp thermodynamic contrast across the frontal inversion allows for nearly complete decoupling between the two layers, which decreases the drag on the overriding air allowing for convective overturning (Colman 1990a).

Elevated storms are commonly found in areas with a local wind maximum. A large number of these storms were found downwind from the max wind region and on the cyclonic shear side of the wind max (Colman 1990a). Looking at a thermodynamic diagram can aid in the assessment of elevated convection, so long as winds are plotted. A common feature of elevated thunderstorms that can be seen is these diagrams is veering winds with height. Elevated thunderstorms tend to occur in environments with stronger winds at the 850 and the 500-mb levels (Colman 1990a). This strong shear suggests that the background environment is baroclinic.

2.3 Climatology of Elevated Convection

Forecasting severe threats from elevated convective thunderstorms is challenging. In order to further understanding of the hazards that can be produced by elevated convection and improve forecasting for these events, it is

important to look at the climatology. Known threats from elevated convection range from heavy rainfall and snowfall, to severe threats including hail, wind, and tornadoes. While forecasting for hail is handled well, the same cannot be said for forecasting severe wind.

Grant (1995) was among the first to do a study of elevated events and he looked at cases in a two-year period between April 1992 through April 1994. 11 cases were selected, based on the criteria given by Colman (1990a) in that they were on the cold side of the analyzed surface boundary and showed a distinct contrast in temperature, dew point temperature and wind direction. The cases chosen by Grant (1995) to be included in this study also had an occurrence of at least five severe storm thunderstorm reports (tornadoes, wind gusts ≥ 50 kt, hail ≥ .75 in) that occur at a location at least 50 miles north of the boundary.

A five-year study was done by Horgan et al. (2007), which examined 129 cases of elevated convection using the same criteria as Grant (1995). Of those 129 events there were 1066 severe storm reports. It was found that 624 (59%) of the reports were hail, 396 (37%) were wind and 46 (4%) were tornadoes. These results are similar to what was found by Grant (1995) being that hail was the dominant threat while tornadoes were relatively rare.

Further expanding on the work of Grant (1995) and Horgan et al. (2007) a 10-year study was done by Market et al. (2019).The criteria used to determine severe weather follows the National Weather Service (NWS) pre 2010, for hail 1.0 cm (0.75 in) wind 25 m s^{-1} (50 kts) or greater and tornadoes. In this study there were 80 cases identified as elevated convection producing severe

thunderstorms. These 80 cases were then classified as either prolific or marginal. Prolific cases are defined as having 5 or more severe reports, and marginal having less than 5 severe reports. There were 1040 total reports of severe weather associated with these 80 cases. These reports followed the pattern found by both Grant (1995) and Horgan et al. (2007). Once again, hail was the most frequently reported type of severe weather (765 [73.5% of all reports]) followed by wind at (261 [25.1%]) and tornadoes (16 [1.5%]). Out of the 80 cases examined all but four had hail 1 inch in diameter or greater.

2.4 Elevated Convection: Severe Weather

As previously mentioned, elevated thunderstorms are capable of producing all forms of severe weather. The studies done by Grant (1995), Horgan et al. (2007) and Market et al. (2017) all confirmed the most common threat from elevated convection is hail, followed by wind, with tornadoes occurring far less frequently. Horgan et al. (2007) found that forecasting for severe hail was handled well, but that is not the case for the other threats. Thus, it is important to identify which parameters could help improve the forecasting of severe wind and tornadoes.

Studies have shown that many severe hail reports often have severe wind reports as well. Identifying what separates the severe wind threat from the severe hail threat is important. It has been found that CAPE values are similar with all three modes of severe weather (Kuchera and Parker 2006). So, using the CAPE parameter alone is not enough to distinguish the type of threat posed

by and elevated thunderstorm. Since wind is the next most prevalent threat, a closer look at what would produce severe wind is necessary.

2.4.1 Severe Wind

While severe wind is not the greatest threat from elevated convective thunderstorms, it does have a significant impact. Approximately 21 deaths and 360 injuries occur yearly in the U.S. that can be attributed to severe convective winds (Kuchera and Parker 2006). This is one of the reasons an improvement to the forecasting of severe winds is needed.

A large number of parameters are used in the forecasting of severe wind. These parameters include ground-relative wind velocity, surface-based lapse rates, CAPE, humidity aloft and lapse rates aloft. Kuchera and Parker (2006) found that ground-relative wind velocity was an effective way to assess the potential for damaging winds. They also found that examining the CAPE, humidity aloft and the lapse rates aloft were moderately effective, while looking at the surface-based lapse rates were ineffective. Severe convective wind events are commonly associated with bow echo systems or derechos due to the moderate to strong shear. However, this is not the only type of storm that can produce strong winds, as any strong downdraft is capable of producing damaging winds.

Downdrafts are a result of evaporative and sublimational cooling, as well as precipitation loading, leading to negative buoyancy. The strength of the downdraft is an important part of determining if severe winds will occur.

Thunderstorms commonly have outflow winds due to this evaporational cooling and precipitation loading that cause the air to be negatively buoyant; it then descends to the surface and diverges. The greater the strength of the downdraft the greater the likelihood severe winds will occur. Evaporative cooling is one of the main forces that effects the strength of the downdraft. To achieve evaporative cooling and get a stronger downdraft, a layer of dry air is necessary. Other factors that enhance the strength of the downdraft include a high liquid water content, small drop size and steep lapse rates (Johns and Doswell 1992). The steep lapse rates allow for the negative buoyancy to continue as the parcel descends towards the surface. Downdrafts do not have to be saturated. If the parcel descends unsaturated then a greater lapse rate is required.

The type of storm present can also impact the factors that can increase the strength of the downdraft. Mesoscale convective systems (MCS) have also been known to produce damaging winds. Downdrafts from the MCS are enhanced when cold pools form as a result of multiple storms' outflows merging (Kuchera and Parker 2006). In addition to contributing to the strength of the downdraft, cold pools can also aid in the re-development of convection. Other factors that can enhance the downdraft include the strengthening of surface winds due to the decent of the rear-inflow jet (Kuchera and Parker 2006). Downdrafts can also be driven by dynamic pressure forces in convection such as the rear-flank downdraft (Kuchera and Parker 2006). As shear and instability increase, pressure gradients and downdrafts intensify, leading to stronger

winds. Kuchera and Parker (2006) found that strong wind fields in the lowest levels contribute to the possibility of damaging winds being produced by an MCS in several ways. First, the downdraft carries momentum from the upper levels to the surface. In addition, the MCS has fast storm motion and increased speed in gust fronts. The last is that the faster wind speeds aloft have higher values of vertical wind shear that may prolong the life of the MCS.

2.5 DCAPE and DCIN

DCAPE is a parameter that has been used primarily in the forecasting of severe wind threats. DCIN is a relatively new parameter and its uses in forecasting continue to evolve. DCAPE and DCIN have been used to determine frontal motion. From there the uses of these parameters evolved into determining whether convection was truly elevated by looking for the presence of a stable layer. The DCIN and DCAPE also improved the forecasting for heavy rainfall and snowfall. The aim now is to use these variables to determine other threats produced by elevated convective thunderstorms such as hail and wind.

DCAPE has been used in previous studies with other variables that contribute to downdraft strength. Kuchera and Parker (2006) used DCAPE paired with WINDINF, which is the wind at the highest positively buoyant level in the surface inflow. The issue with this method is that it includes variables also used for hail and tornadoes, so it is difficult to determine precisely what threat will occur. In the study done by Kuchera and Parker (2006) CAPE and DCAPE were used to evaluate the instability. It was also found that sounding

parameters, such as wind speed and shear, proved useful in forecasting severe convective winds.

In the study done by Horgan et al. (2007) it was found that severe winds often occurred with severe hail, but not always. There were twice as many hail only cases versus wind only cases (Horgan et al. 2007). This study posed the question, is the environmental stable layer relevant to severe wind at the surface? This work showed that not only is the stable layer a factor in severe winds at the surface, the DCAPE/DCIN ratio is a useful tool in determining just how much the stable layer affects severe winds at the surface. Factors that contribute to severe wind at the surface include: the strength and depth of the inversion, i.e. the stable layer, the strength of the winds above the inversion, and the relative humidity above the inversion. DCIN can be used as a measurement of the depth and intensity of the inversion (Market et al. 2019). In addition to this DCIN is limited to saturated parcels whose descent relies upon sublimation/evaporation (Market et al. 2019). This is why the relative humidity above the inversion is important-- dry air above the inversion aids in the likelihood of severe winds reaching the surface.

2.6 Parcel Level

The level from which a parcel is lifted is important to get an accurate look at the instability of the environment. It is known that both CAPE and CIN values depend on which level the parcel is lifted from. There are several approaches to selecting a parcel to lift: a surface-based parcel, a parcel that represents the average conditions of the lowest 100-mb layer, and the most

unstable parcel in the lowest 300-mb layer. The third approach is more appropriate when evaluating elevated convection (Rochette et al. 1999).

θ_e represents an important parameter when evaluating elevated convection. This quantity can be useful in determining the slope and position of a front, as well as identifying layers of convective instability and finding the most unstable parcel (Moore et al. 1998). When lifting a parcel with the highest θ_e in the lowest portion of the atmosphere the results are typically increased values of CAPE. In addition, choosing this level from which to lift a parcel can reveal an unstable thermal environment that would be missed when computing CAPE by lifting a surface-based or average parcel (Rochette and Moore 1996).

While it would appear that using the most unstable parcel (with the highest θ_e value) to compute CAPE and CIN would yield the best results, it is unclear if this same method would provide similar results for DCAPE and DCIN. A study was done by Market et al. (2019) to assess the impact of heights on descending parcel origin. This study had 80 cases broken down into two categories: prolific (five or more severe reports) and marginal (fewer than five). There were 55 significant cases and 25 marginal cases. Multiple levels were analyzed, ranging from 0.3 km to 6.4 km AGL. The box-and-whiskers plots in Fig 2.1.a.b shows the results of this study. It found that regardless of parcel origin height the DCIN remained largely unchanged and followed the same moist adiabat. It was found that DCAPE decreases as level above ground decreases, increasing the magnitude of DCAPE. The minimum θ_e yields the

best results for evaluating severe winds at the surface. This approach gave values of DCAPE being much greater than the values of DCIN.

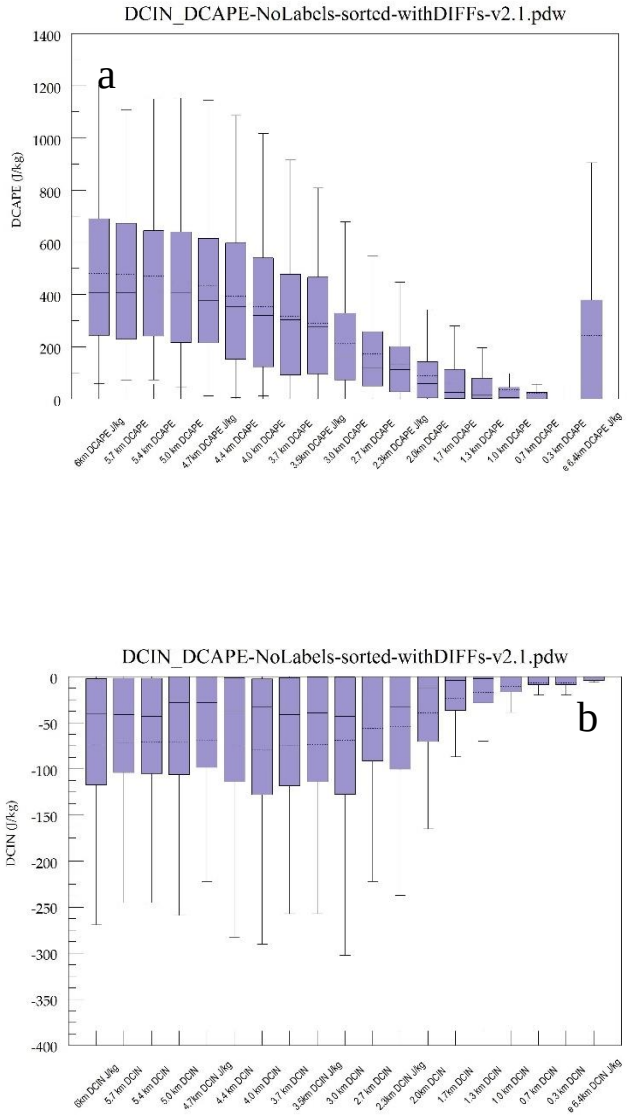

Figure 2.1. Box-and-whisker plots of thermodynamic variables (DCAPE(a), and DCIN(b); J kg^{-1}) of elevated thunderstorms for multiple levels.

2.7 Gravity Waves and Elevated Convection

Gravity waves are commonly found in the atmosphere with elevated convection. This is due in part to the preferred environment for gravity waves being in the cold air north of a surface frontal boundary (Bosart and Seimon 1988). Since this is also one of the requirements for elevated convection, it comes as no surprise that gravity waves and elevated convection are often found together. Gravity waves can also be excited downstream of jet cores with high velocity where divergence is increasing and the Rossby number is large (Bosart and Seimon 1988). While gravity waves and elevated convection often appear together it does not appear that gravity waves alone can initiate convection (Colman 1990b). Rather it is thought that gravity waves are a result of convection. Deep convection could be a source region for gravity waves. From this deep convection a gravity wave forms and propagates away from the area of convection (Bosart and Seimon 1988).

Some of the mechanisms responsible for the formation of gravity waves are similar to those of elevated convection, specifically, the vertical shear instability, which amplifies the wave, overturns it, then breaks down into turbulence. Another important factor in gravity waves is geostrophic adjustment (Bosart and Seimon 1988). One way to examine this geostrophic adjustment is to look at the ratio of absolute horizontal divergence to absolute vorticity (Bosart and Seimon 1988). Convection plays a role in the organization and intensification of gravity waves. This is due to the subsidence left behind the

convection as a results of a cold stable boundary layer of air (Bosart and Seimon 1988).

There is a relationship between large amplitude gravity waves and damaging surface winds, rapid pressure changes and intensification of precipitation. Heavy precipitation often precedes pressure falling. Pressure drops of 5 mb or greater have been noticed with gravity waves (Bosart and Seimon 1988). It is after the pressure drop that strong winds at the surface typically occur. This presence of gravity waves interacting with elevated convection increases the amount of momentum transported downward, aiding in the likelihood of the downdraft penetrating a stable layer and reaching the surface to produce damaging winds. It is because of this increased transfer of downward momentum that the presence of gravity waves could aid in the forecasting of severe winds at the surface.

CHAPTER 3. DATA AND METHODOLOGY

3.1 Data Sources

Multiple data sources were used throughout this study. This work includes an analysis of storm reports, upper air and surface maps, radar imagery, thermodynamic diagram data as well as meteorograms. Storm reports and upper air and surface charts were obtained through the Storm Prediction Center (SPC). Model solutions were obtained from the National Oceanic and Atmospheric Administration (NOAA) Model Archive and Distribution System (NOMADS) to generate skew-T's. Rapid Update Cycle (RUC) and The Rapid Refresh (RAP) model analysis output were obtained from the NOMADS site and used in this study in creating soundings and the calculating DCAPE and DCIN. Radar imagery used in this study were retrieved from the National Center for Environmental Information (NCEI). The meteorograms used to display pressure and wind speed were obtained through the Plymouth State University Weather Center.

3.1.1 NCEI and SPC

The SPC was the main source in this study for gathering storm reports, showing how many wind reports there were associated with the storm of interest, as well as obtaining upper air and surface charts. The upper air and surface charts were used to ensure the storms evaluated in this research met

Colman’s criteria for elevated thunderstorms. The storm reports were used to verify that severe winds did occur at the time and location of study.

The NCEI was used to gather radar data associated with the elevated thunderstorm. These data were downloaded then ran through GR Analyst to produce the radar imagery shown. Reflectivity images were shown to examine the location of the storm, and base velocity was used to determine the wind speed and direction. The main use of the radar data was to help assess the presence of gravity waves, as well as to determine the locations along the storms' paths where the severe wind reports occurred.

3.1.2 RAP and RUC

For the third case study the RUC model was used to generate proximity sounding data. This is due to the fact that the date of the third case study was before 2012, when The RUC was replaced by the RAP model. RUC has 20-km horizontal grid spacing and 50 vertical levels. In 2005, the RUC was enhanced with a 13-km horizontal grid spacing (Benjamin et al. 2016). Since the case that uses the RUC model occurred in 2011, the 13-km horizontal grid spacing was used in this study. The RUC was shown to be more accurate in short-term forecasting when more observations were ingested into the model (Benjamin et al. 2016).

RAP is the successor of the RUC. The RAP began operation in 2012 and was used for the rest of the cases in this study. Due to the quick processing time

of the RAP, it was more efficient in forecasting the short-term and providing situational awareness. Some of the changes from the RUC to the RAP included improved model statistics and grid-point statistical interpolation analysis system (Incorporating additional data with higher assimilation frequency, Benjamin et al. 2016).

The use of the RUC and RAP models was highly beneficial to this work due to the hourly analyses they provide. The use of hourly analyses allowed for the construction on skew-T's that were used to analyze the pre-storm environment, conditions during the storm, and the post-storm environment. Skew-T's were created by first accessing the model solutions from the NOAA Model Archive and Distribution System (NOMADS). From there the 13-km RAP or RUC data were downloaded and converted from a GRIB file to a General Meteorology Package (GEMPAK) file. Once the file was converted it was run through the NSHARP program to create a text file skew-T for the specific latitude and longitude relevant to the case studies. From there the text file was then run through ROAB^{TM}, a commercially available sounding analysis, DCIN and DCAPE were then calculated by an algorithm in the software that uses the coldest wet-bulb temperature in the lowest 6 km from which the parcel begins to descend.

3.2 Calculating DCAPE/DCIN

For this study, DCAPE developed by Gilmore and Wicker (1998) was used (Eq 1.1). DCAPE generally represents the convective energy available to a

downdraft as a result of negative buoyancy. However, when a sinking parcel passes through an inversion layer near the surface it becomes positively buoyant, due to the parcel becoming warmer than the environment (Market et al. 2107). Market et al. (2017) proposed a way to quantify the positive area in the subinversion layer and therefore counteract the negative buoyant effects of the downdraft parcel when it hits this layer

For all the case studies in this work, the calculations for the DCAPE and DCIN were performed through the ROAB^{TM} software. As previously mentioned, this program uses an algorithm that uses the coldest wet-bulb temperature in the lowest 6 km to determine the initial level from which the parcel descends to compute DCAPE and DCIN. The RUC and RAP were used to obtain the output, then the RAOB software was used to establish the pre-hour vertical environmental profile with quantified thermodynamic variables (DCAPE and DCIN) to show the environment at the storm's location. Multiple soundings were used for each case study. The idea is to show the pre-storm environment, the environment at the time of the severe weather occurring, then the environment after the severe threat has passed. The first two case studies focused on the environment from one location. The third case study was over the evolution of the storm, so a more expansive view was used by selecting four different locations along the path of the storm.

3.3 Case Selection Criteria

Three cases were analyzed in this study. It is recognized that this is a small sample size. Certain criteria were used in each case to determine if the case fit the needs of the study. For each case severe storm reports from the SPC were gathered to determine what type of severe weather was present. A report was considered to be severe using the NWS pre-2010 criteria for severe weather of hail with diameters of at least 0.75 inches, wind speeds of 50 knots or greater, or tornadoes. Two out of the three cases did have severe wind reports. In addition to this criterion, upper air charts and surface maps were used to determine if the storm fit the criteria for elevated convection. Each case fit Colman's(1990a) criteria for elevated frontal convection with the location being 50 statute miles north of the cold front. In addition, the temperature, dewpoint, and wind were similar in the areas surrounding the chosen location.

In addition to the common criteria above, each case also had unique factors that influenced the selection for this study. The first case was chosen due to the application of the |DCIN/DCAPE| ratio used by NWS employees in issuing a severe thunderstorm warning. The real time use of this ratio made this case ideal for this work. The second case included an analysis of a meteotsunami that impacted Lake Michigan. Another factor that played a role in selecting the second case was a 60-knot wind vector change that occurred, which will be discussed in greater detail in section 4. The third case was chosen based on the transition from severe hail reports being the dominant threat, then switching to

severe wind being the threat. This pattern has been recognized as a common occurrence with elevated convection, so this case was selected to see if there was a relationship between the transition and the |DCIN/DCAPE| ratio.

CHAPTER 4. RESULTS

This chapter will include an in-depth analysis of each of the three case studies chosen for this work. The analysis will include a look at the synoptic conditions for each case, as well as severe storm reports and unique factors associated with the case, which aided in the selection of each case for this work. Common features that will be analyzed form each case include upper-air and surface charts, storm reports and skew-T diagrams for the purpose of evaluating the values of DCAPE and DCIN. In addition, the first two cases also have plots of the |DCIN/DCAPE| ratio. These plots are used to highlight the area most likely to see severe winds at the surface.

4.1 Case 1: An Overview

On 06-07 February 2019, the state of Missouri experienced multiple forms of hazardous weather. In northwest and central Missouri there was an ice storm present, the eastern portion of Missouri was experiencing flooding, and the southern portion of Missouri was affected by severe thunderstorms and tornadoes. The area of interest in this case is southwest Missouri, where Springfield is located. This hazardous weather occurred over a two-day period, 06-07 February 2019. In this case the time of interest is between 0300 UTC and 0900 UTC on 07 February 2019, with particular attention being paid to the time between 0500 UTC and 0600 UTC when the first reports of severe winds at the surface were recorded.

A slow-moving frontal boundary, responsible for the ice in the north and thunderstorms in the south, progressed through Springfield, Missouri, between the hours of 0300 UTC and 0900 UTC 07 February 2019. Associated with this front was a bow echo. Bow echoes are associated with two different synoptic patterns, the first being a warm season pattern and the second being a dynamic pattern (Johns and Doswell 1992). This bow echo was of the second variety, that being a dynamic pattern. This pattern is most commonly associated with bow echoes that form as a result of a squall line being present. There is typically a strong low-pressure system associated with this dynamic pattern (Johns and Doswell 1992). These bow echoes are typically located slightly to the right of the mean flow, as was the case in this study.

This case was unique in the fact that there was elevated convection associated with this boundary that produced all manner of severe weather including tornadoes as shown in Fig 4.1.

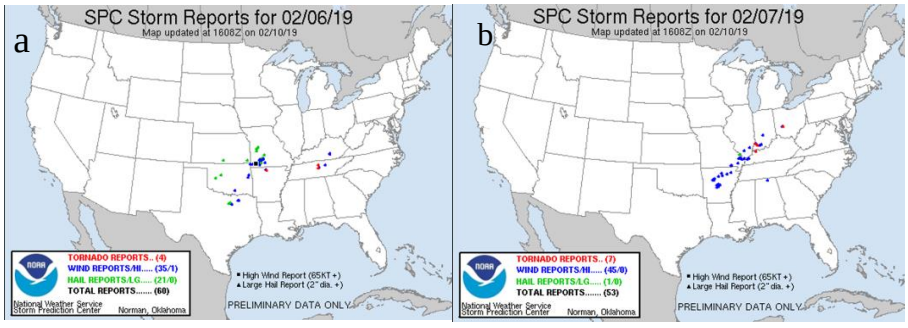

Figure 4.1. Storm reports from SPC for a) 06 February 2019, and b) 07 February 2019. Blue dots represent wind reports, green dots represent hail reports, red dots represent tornado reports, and the black square represents a wind report of at least 65 kt.

Figure 4.1.a illustrates the number of severe wind reports from this system located in and around the area of interest. It also shows that as the storm progresses to the northeast, wind reports increase while hail reports decrease. As previously mentioned, this is a common theme seen in the case of elevated convection and will be examined further in case 3.

4.1.2 Case 1: Analysis

Upper-air and surface analyses were performed to ensure that this case fit the criteria proposed by Colman (1990a.) for elevated frontal convection. Figure 4.1.2 shows the position of the front at the specific time of interest. The figure also shows broad southwesterly flow was present in the mid-troposphere, ahead of a deep shortwave trough over the Intermountain West. Severe convection with wind gusts as strong as 60 knots were associated with this boundary. Multiple instances of wind damage occurred near and north of the analyzed frontal boundary within 15 miles of the Springfield, Missouri, Automated Surface Observing Station (ASOS).

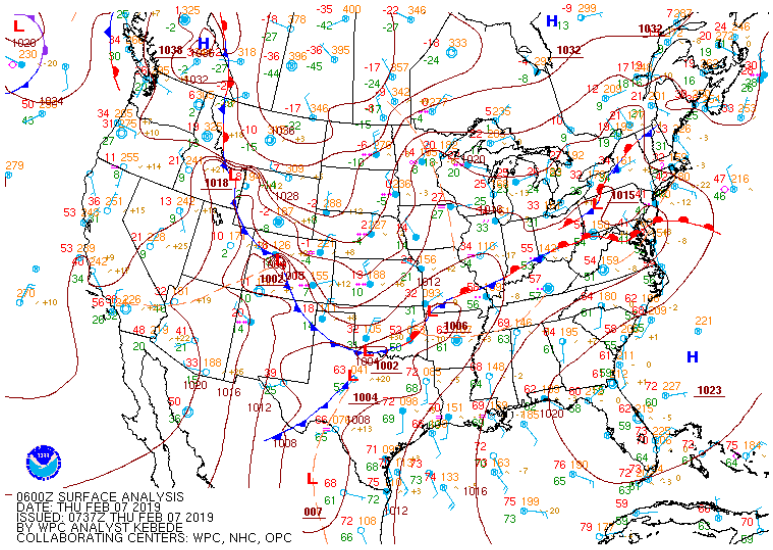

Figure 4.1.2: Surface analysis valid at 0600 UTC 7 February 2019. Brown solid contours are isobars (mb). Station models, fronts, and other boundaries are depicted using standard symbology.

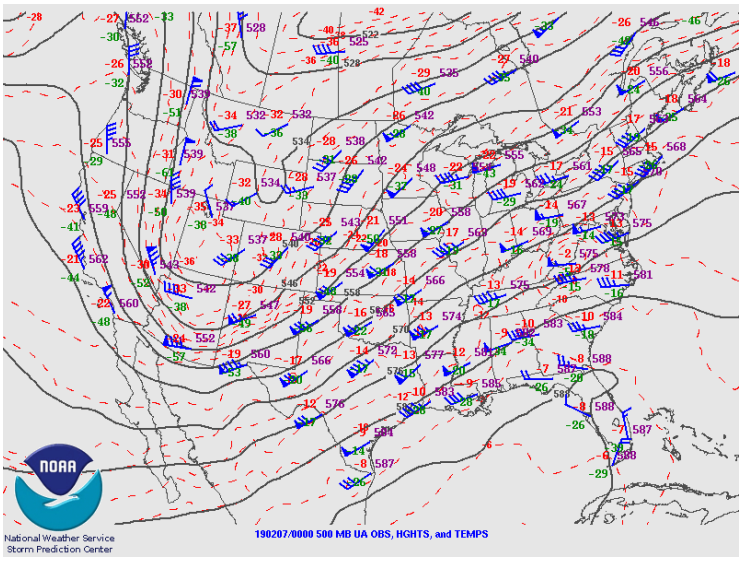

Figure 4.1.3: 500-mb analysis valid at 0000 UTC 7 February 2019. Solid black contours are geopotential heights (dkm) and red dashed contours are isotherms (deg C). Station model data are depicted using standard format.

Figure 4.1.2 shows that this case fits Colman's (1990a) criteria for elevated convection in that this system was north of the front. Figure 4.1.3 shows that

Springfield is located in the upstream flow at the 500-mb level. This puts Springfield in the preferred location for maximum divergence.

An additional data source that proved to be extremely helpful when analyzing this case is the meteorogram shown in Fig 4.1.4. This figure shows temperature, current weather, visibility, wind speed and direction, cloud height, and pressure. Focusing specifically on wind direction in Fig 4.1.4 it is evident that there is a wind shift leading up to and during the specific time of interest.

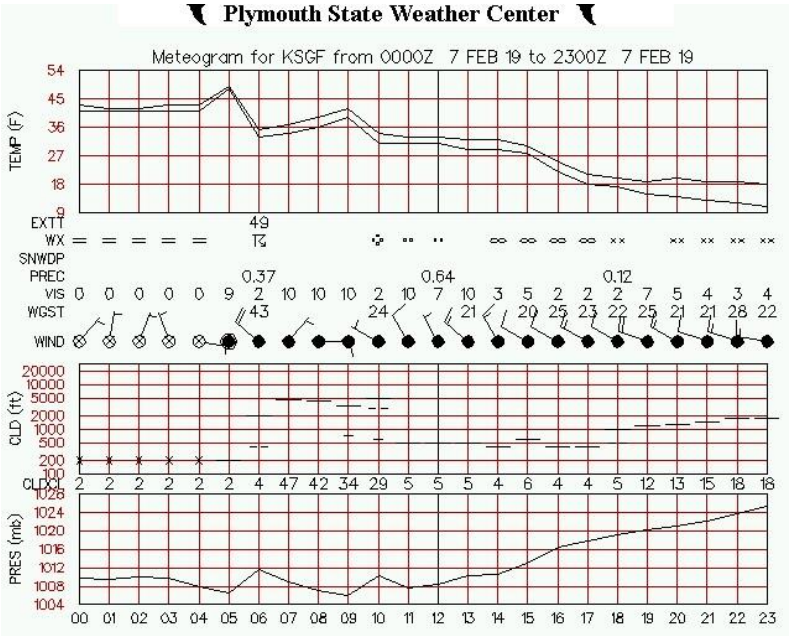

Figure 4.1.4: Meteorogram for Springfield, Missouri (KSGF), valid from 0000 UTC to 2300 UTC 07 February 2019 (Courtesy Plymouth State Weather Center).

Starting at 0300 UTC the wind direction is from the north. At 0400 UTC the wind then shifts to out of the east, before shifting back to northwesterly at 0600 UTC. This shows that there was a wind shift just ahead of the change in precipitation. Fig 4.1.4 shows the weather conditions at the time of this wind shift go from mist (represented by the = sign) to thunderstorm.

What Fig 4.1.4 fails to capture, however, is the dramatic wind shift between the hours of 0500 UTC and 0600 UTC that occurred. This can be seen in Fig 4.1.5 which is a meteorogram from a home weather station in Republic, Missouri (an employee of the National Weather Service Springfield office). This figure better captures the wind shift that occurred in the hour leading up to the severe wind. Fig 4.1.5 show that winds start out northwesterly before the passage of the bow echo, while on the cold side of the front. From there, winds shift to a strong southwesterly flow, then a mere 15 minutes later return to a north-northwesterly flow. In addition, there is a sharp temperature drop that occurs after this wind shift, followed by a spike in temperature on the cold side of the front.

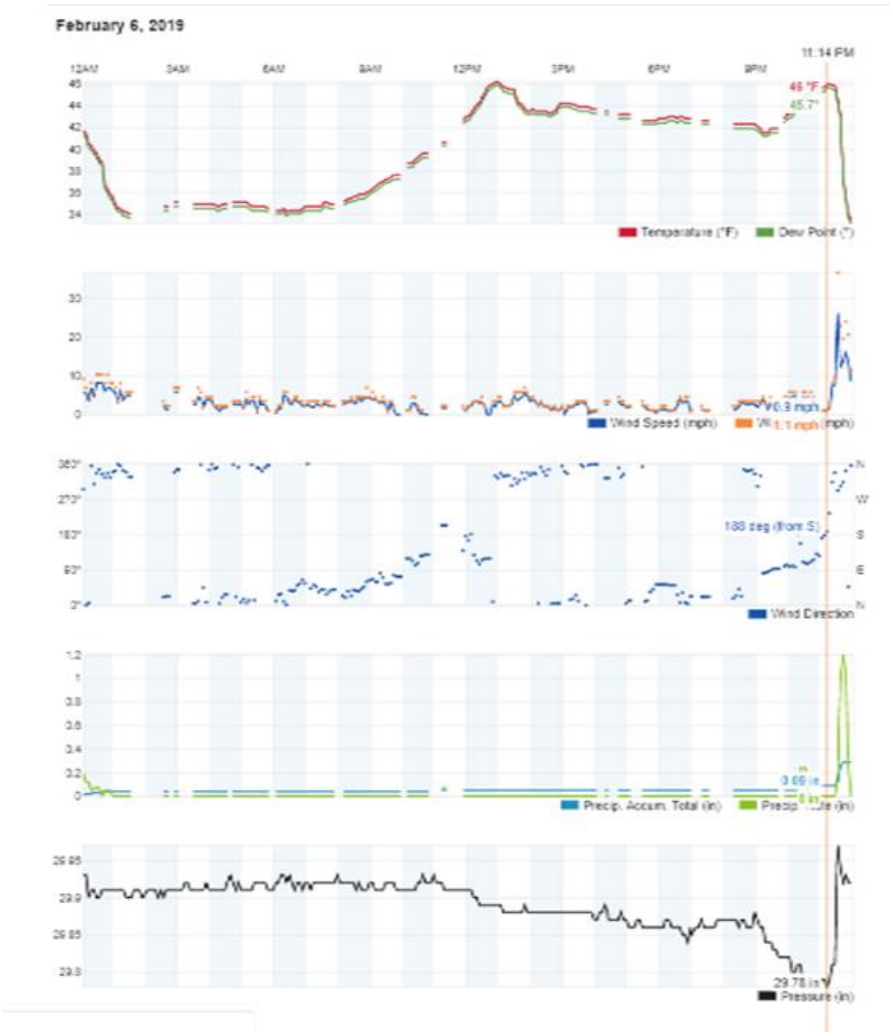

Figure 4.1.5: Meteorogram from Republic, Missouri, showing temperature and dew point, wind speed and direction, precipitation accumulation, and pressure, valid for 0000 CST to 2359 CST 06 February 2019. The brown vertical line represents the time of interest 11:14pm.

Another point of interest is the change in pressure. At 0300 UTC 7 February 2019 (2100 CST the previous day) the pressure is 1010mb, from there it slowly drops until 0500 UTC 07 February 2019 (2300 CST the previous day) when it reaches a minimum of 1006 mb. It is noteworthy that the time of the pressure drop coincides with the time of the spike in temperature. Fig 4.1.4 shows a sharp increase in the pressure between 0500 and 0600 UTC 7 February 2019.

The pressure rises from 1006 mb to 1012 mb. This increase in pressure of approximately 6 mb over the course of an hour lead to further analysis of pressure data. One-minute pressure data was analyzed after noting the pressure behavior show in Fig 4.1.4. The analysis of this one-minute pressure data suggested there were gravity waves present that were possibly aiding in the strength of the winds at the surface. The presence of gravity waves will be discussed in further detail later in this section.

The next analysis that will be discussed in this section is the sounding data that provides the values of DCIN and DCAPE. The sounding data used in this case is real time data obtained by weather balloon launches done by the NWS office in Springfield. The 0600 UTC balloon was launched in a pre-convective environment just ahead of the strong winds that would impact the Springfield area.

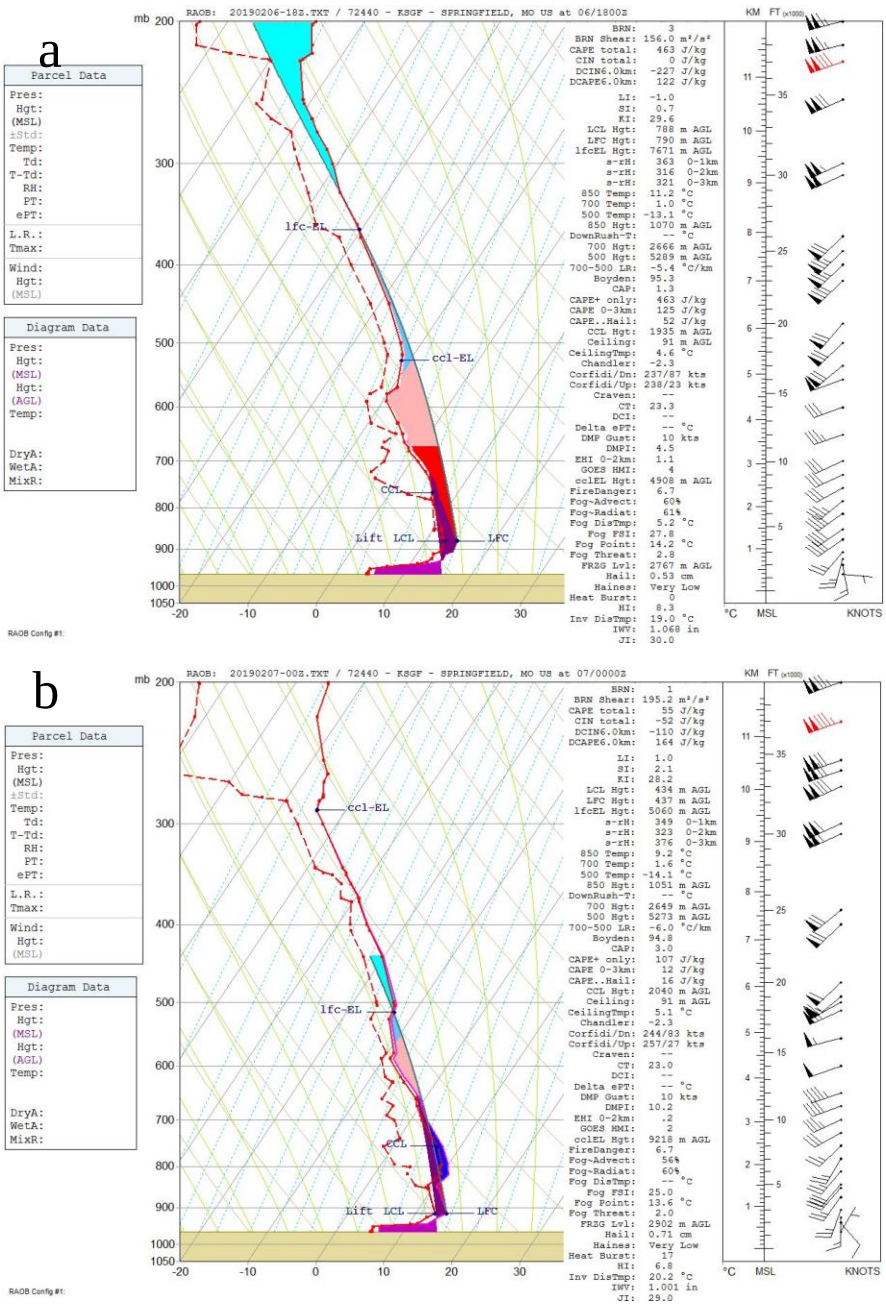

Figure 4.1.6: Soundings from Springfield, Missouri (KSGF), showing DCIN and DCAPE values at a) 1800 UTC 06 February 2019, b) 0000 UTC 07 February 2019, c) 0600 UTC 07 February 2019, d) 1200 UTC 07 February 2019. The DCAPE is represented by the dark purple shading. DCIN is represented by the light purple shading.

c

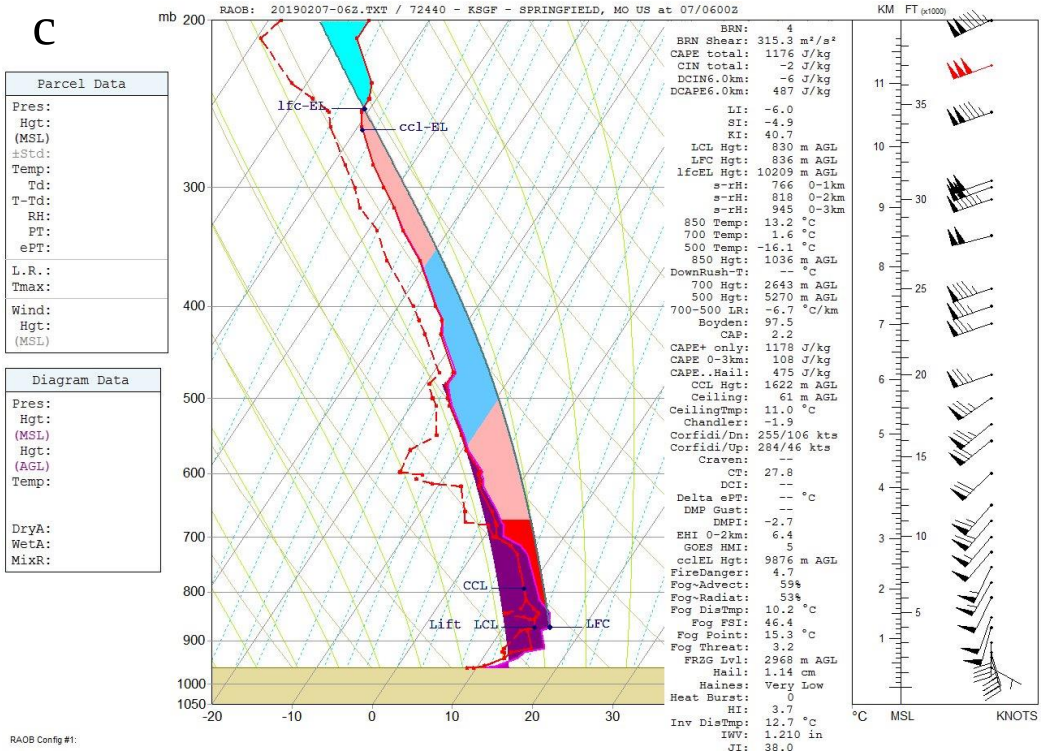

d

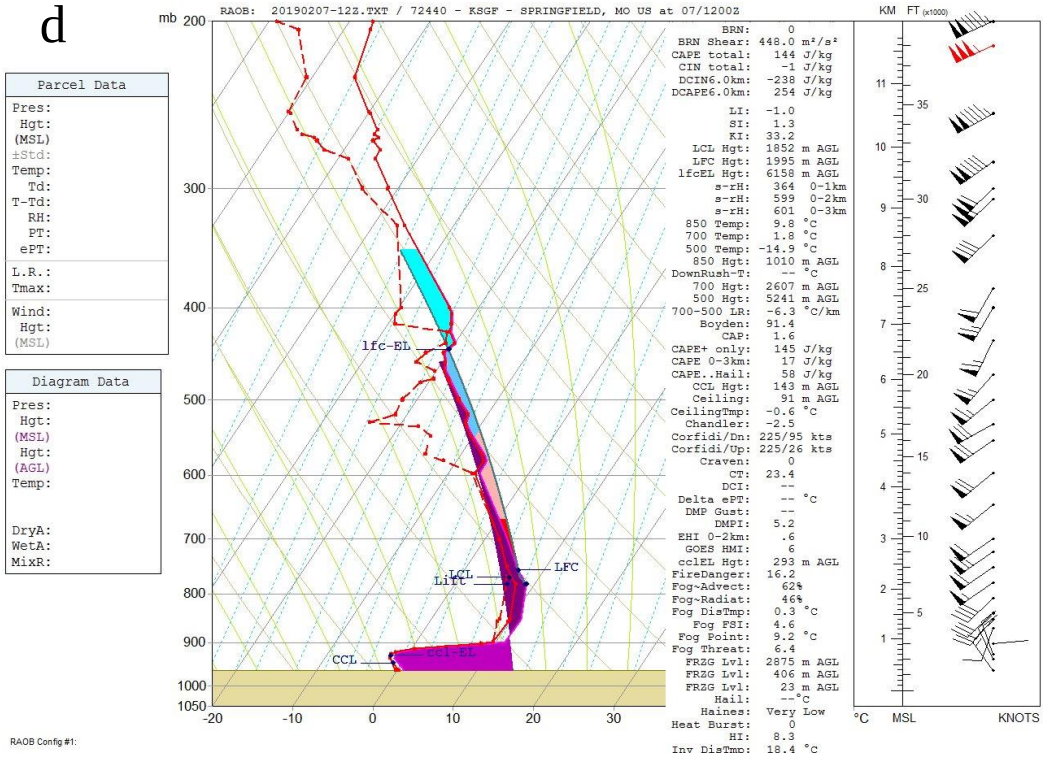

Figure 4.1.6: Continued

The values for DCIN and DCAPE can are illustrated with the dark purple color representing DCAPE and the light purple representing the DCIN. Multiple soundings were analyzed to identify a trend in the values of DCIN and DCAPE and to examine the evolution of the storm and to determine how these values change as the storm progressed. Figure 4.1.6 shows a steady decrease in DCIN and steady increase in DCAPE leading up to and at the time of the severe wind reports. The sounding for 1800 UTC on for 06 February 2019 shows values of 6-km DCIN at -227 J kg^{-1}. DCAPE values at this time, also 6-km, were 122 J kg^{-1}. The sounding for 0000 UTC on 07 February 2019 had DCIN values of -110 J kg^{-1} and DCAPE values of 164 Jkg^{-1}. The sounding at the time of the event (0600 UTC) shows values of DCIN at -6 J kg^{-1} while values of DCAPE are 487 J kg^{-1}. This would provide a ratio of near zero for |DCAPE/DCIN|. These data support the hypothesis that a ratio of near zero would allow for winds to penetrate a stable layer and produce severe criteria winds at the surface. The final sounding shown in Fig 4.1.6 is for 1200 UTC, after the line has progressed out of the area. This sounding shows values of DCIN at -238 J kg^{-1} and values of DCAPE at 254 J kg^{-1}. This sounding has the ratio near one, which according to the hypothesis, suggest the threat for severe wind has passed. The |DCAPE/DIN| ratio was used in real time by forecasters and that contributed to the decision to issue a severe thunderstorm warning for the area.

Another visual representation of the |DCAPE/DCIN| ratio, and the threat of severe winds at the surface, is Fig 4.1.7.

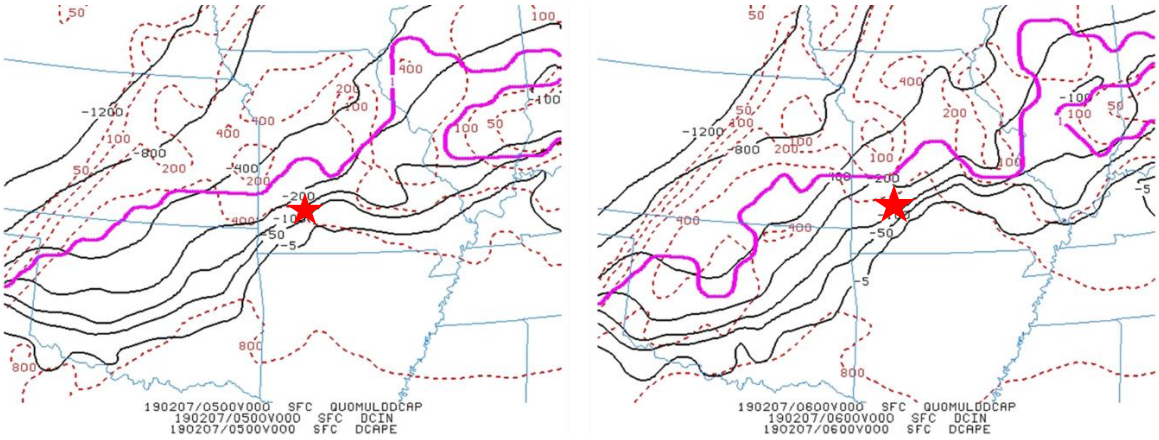

Figure 4.1.7. RAP initial analyses of DCIN (solid black, J kg-1) and DCIN (dashed red, J kg-1) valid at a) 0500 UTC and b) 0600 UTC 07 February 2019. The purple line represents a DCIN/DCAPE ratio near 1, and the -5 contour for DCAPE represents the zero DCIN/DCAPE ratio. The red star represents the location of Springfield, Missouri.

This plot is helpful in narrowing down the area that is at greatest threat for experiencing severe surface wind. Fig 4.1.7 visually represents the "Danger Zone" showing the area at greatest risk for severe winds at the surface. The area between the purple line and the -5 DCAPE contour is the area more likely to experience those severe winds at the surface.

4.1.3 Case 1: Gravity Wave Presence

Another point of interest in this case was the clear presence of gravity waves.

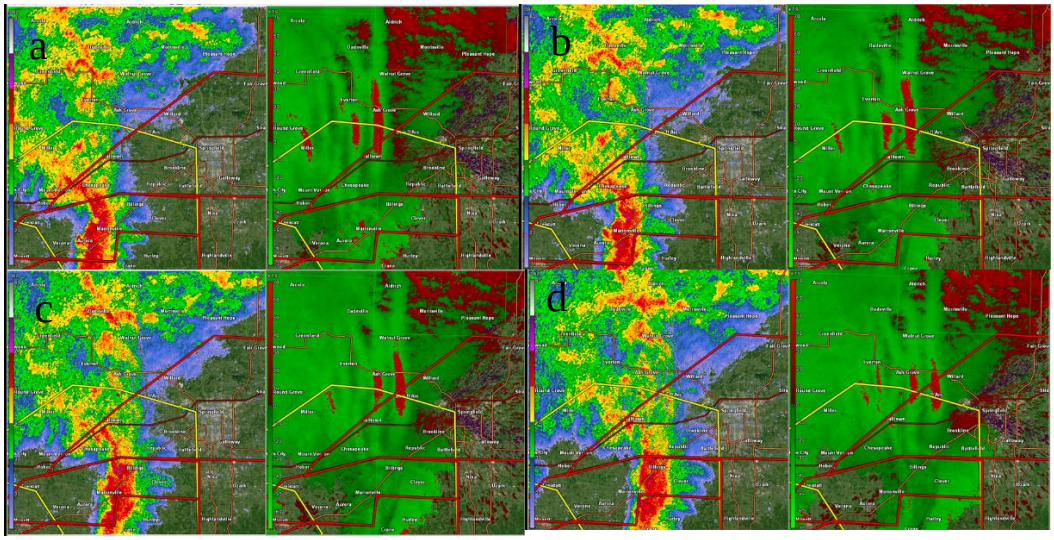

Figure 4.1.8: 0.5 degree base reflectivity (dBZ, left) and base velocity (kt, right) from the Springfield, MO (KSGF) WSR-88D valid at a) 0525 UTC, b) 0527 UTC, c) 0530 UTC, and d) 0532 UTC 07 February 2019, a) 0525 UTC, b) 0527 UTC, c) 0530 UTC, d) 0532 UTC

Fig 4.1.8 shows both the reflectivity and the base velocity of the line as it approached the Springfield area. The reflectivity is used to show the location of the bow echo. The images to note are the base velocity images. These images show the clear presence of gravity waves just to the north and in front of the bow echo. Fig 4.1.8 shows four well defined gravity waves. It was determined there was a gravity wave approximately every four minutes, traveling at a speed of 47.3 knots. The speed the gravity wave was moving was calculated by measuring the distance the wave traveled divided by the time it took to travel that distance. From there an assessment of the impact of the gravity wave was done using the method from Schneider (1990). The first step was to calculate the Brunt-Vaisala number using the formula:

$$N = \sqrt{(\frac{g}{\theta})(\frac{\partial \theta}{\partial z})} \qquad \text{(Eq 4.1)}$$

Where g is the acceleration of gravity, θ is the potential temperature at the height of the inversion, and z is the height of the inversion. This calculation was performed to determine the frequency with which the waves were traveling. The frequency was calculated using multiple levels. In one case using the lowest level, which was stable, it resulted in a frequency of a gravity wave every 11 seconds. The layer of the inversion was then used in the same calculation and yielded results of a gravity wave every 27 seconds. These results did not match what was calculated from the observed radar data. One explanation for this could be the beam height of the radar. These gravity waves occurred close to the radar and at a lower level in the atmosphere. The calculations for the gravity waves were done at levels that were higher in the atmosphere. This could explain the faster frequency of the gravity waves that was calculated versus the calculations from the observed data.

In addition, a Fourier transform was performed for the one-minute pressure data. The first attempt focused on the hour between 0500 and 0600 UTC. The results were conclusive and did not pick up the wave signal. A second Fourier transform was performed for a longer time period, this one from 0400 to 0700 UTC. Increasing the time period did not change the results. The wave signal was not statistically significant.

It is hypothesized that the presence of these fast-moving gravity waves aided in the downward momentum transfer from this storm, contributing to damaging winds at the surface. While this is far from conclusive, the theme of gravity waves being present is one that exists in multiple cases of elevated

convection. The next case that will be analyzed also has gravity waves present, though not as clearly captured by radar as this case. While these gravity waves seem to be a common theme with elevated convection, there was no definitive proof that they impacted the winds penetrating the stable layer.

4.1.4 Case 1: Summary

On 06/07 February 2019, a slow-moving frontal boundary moved through the Springfield area. This system brought severe weather in the form of strong winds and tornadoes. The |DCIN/DCAPE| ratio provided a value near zero, which indicated that severe winds were likely at the surface. The |DCIN/DCAPE| ratio was used in real time by NWS employees, and proved to be a useful tool to make the decision to issues a severe thunderstorm warning for the area. In addition, an analysis of gravity waves that were present at the time of the severe wind reports was done to determine if they had any impact on aiding the downward momentum transport that contributed to the severe winds. This case supports the hypothesis, that is when the |DCIN/DCAPE| ratio is near zero, severe winds can occur at the surface.

4.2. Case 2: An Overview

This case occurred on 13 April 2018. A warm, quasi-stationary front with elevated convection was present. This extratropical cyclone was responsible for

the significant wind experienced across the upper Midwest and into the Upper Peninsula and northern portions of Lower Michigan. At the time of this event Lake Michigan was experiencing record high water levels. This in combination with the significant wind led to the formation of a meteotsunami. This case will focus on two locations: Green Bay, Wisconsin, where the primary threat from the storm was hail, and Ludington, Michigan, where some damage from the meteotsunami was observed.

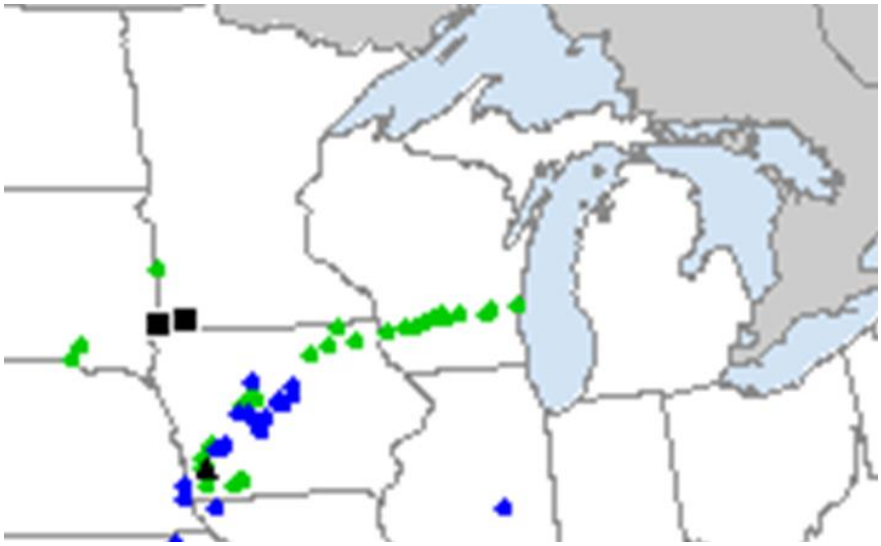

Figure 4.2.1: Storm reports from Storm Prediction Center valid for 13 April 2018. The green represents severe hail reports, the blue represents severe wind, the black squares represent wind reports of at least 65 kt, and the black triangle represents hail of at least 2 inches in diameter.

The time of interest in this case is between 1300 UTC and 1800 UTC 13 April 2018, with particular attention being paid to the 1600 UTC hour. The 1600 UTC hour is when the pressure oscillations and the wind speed peaks occur. One thing to note about this case is Fig 4.2.1. This figure shows the storm reports and clearly there are no severe wind reports for Michigan. That is

because winds did not reach severe criteria. Nevertheless, there was damage observed, due to the wind and the meteotsunami.

This case also featured the presence of gravity waves. These gravity waves were slightly more difficult to determine as the radar did not catch them as clearly as in the previously described case. Again, the interaction of gravity waves with elevated convection will be explored as well to see what, if any, effect the gravity waves might have had on the intensity on the meteotsunami.

4.2.1: History of Meteotsunamis and the Great Lakes

The term meteotsunami is not as well known in the field of meteorology as the term seiche. Therefore, it is important to define the two, so the difference is better understood. A seiche refers to a basin-scale water level oscillation that focuses primarily on the change in water level. A meteotsunami propagates shallow water waves which exhibit many similarities to seismic tsunamis but are generated by a moving atmospheric disturbance (Bechle et al. 2015). meteotsunamis are also on a sub-basin scale. The main difference between a seiche and a meteotsunami is that the seiche focuses on the change in water level, is wind driven and has a duration of greater than two hours, whereas a meteotsunami is mainly driven by pressure oscillations and has a duration between two minutes and two hours.

Meteotsunamis are actually quite common in the Great Lakes, averaging approximately 100 a year. Meteotsunamis are typically associated with convection. They can be caused by a few different events including,

atmospheric pressure and wind perturbations, frontal passage, cyclones, atmospheric gravity waves, and mesoscale convective systems (MCSs). Gravity waves are one of the main contributors to the occurrence of meteotsunamis, due to the pressure changes and the horizontal wind changes (Bechle et al. 2015). The periodicity of meteotsunamis can vary between two minutes and two hours (Bechle et al. 2016). While these are commonly caused by atmospheric disturbances, meteotsunamis can also be a result of reflections in an enclosed basin (Bechle et al. 2016). Of the Great Lakes, Lake Michigan and Lake Erie have the most frequent meteotsunamis. This is due to the water levels playing a critical role in the presence of and damaged cause by meteotsunamis (Bechle et al. 2016). Fig 4.2.2 demonstrates the typical water level of Lake Michigan and is used to provide an example of the deeper parts of the lake, versus the shallower parts. As previously mentioned, Lake Michigan was experiencing record high water levels during this event. So, Fig 4.2.2 is shown mainly for a reference point than for the actual depths of the lake.

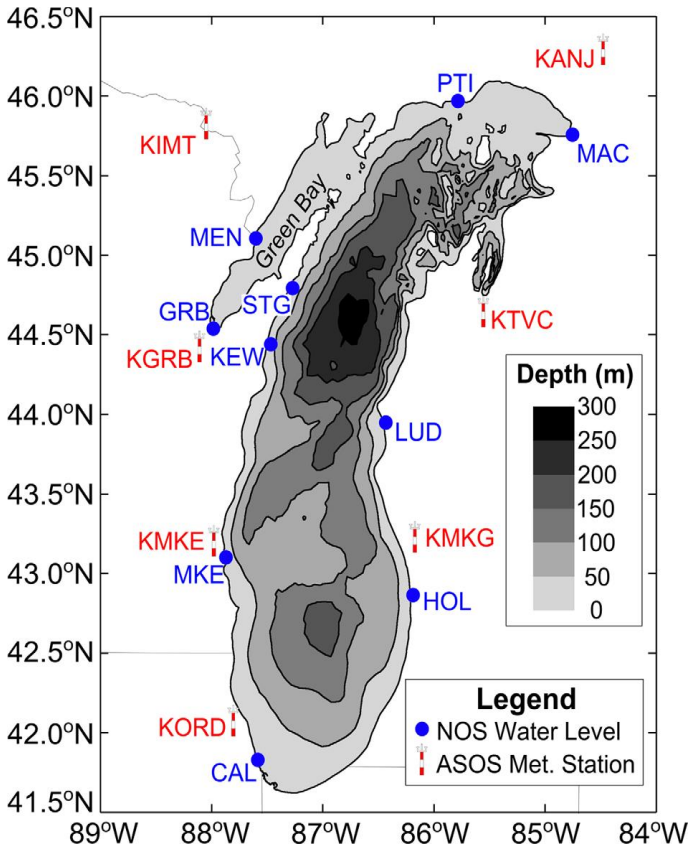

Figure 4.2.2: Lake Michigan bathymetry and locations of NOAA-NOS water level and NWS-ASOS surface meteorology stations (Bechle et al. 2015).

There are two types of meteotsunamis that are discussed in detail in Bechle et al. (2015). The first type is non-trapped long waves. These can be described by Proudman resonance, which shows the atmospheric disturbance propagates with speed U approximately equal to non-dispersive long-wave phase speed:

$$C_{long} = \sqrt{g * Water\ Depth} \qquad \text{(Eq 4.2)}$$

The second type of meteotsunami is the trapped edge waves that propagate parallel to the coast and is amplified by the Greenspan propagation resonance, which says there is a positive correlation between the speed and the

wavelength. The more commonly experienced meteotsunami type for the Great Lakes is the first type, the one cause by atmospheric disturbances.

There is a seasonality to the occurrence of meteotsunamis. Since they are linked with convection, they typically occur in late spring and early summer. This convection accounts for 60% of meteotsunami occurrences (Bechle et al. 2016).

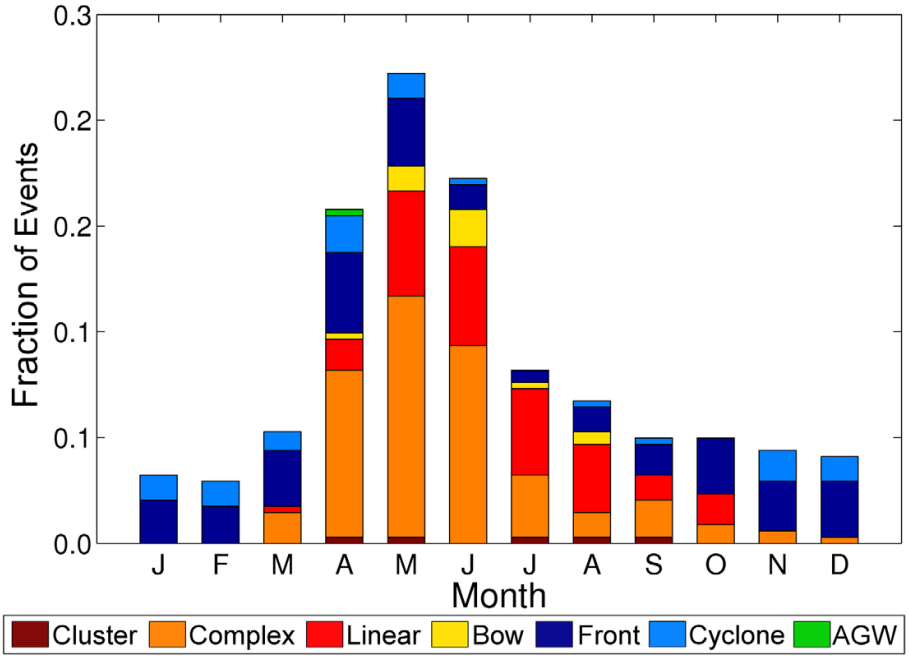

Figure 4.2.3: Monthly distribution of storm structures associated with meteotsunamis aggregated across all stations (Bechle et al. 2015).

This seasonal pattern can be seen in Fig 4.2.3, which shows not only the months with the higher activity, but also the breakdown of what type of storm contributes to the occurrence of the meteotsunami in what month. During the peak season for meteotsunamis it can be seen in Fig 4.2.3 that complex and linear convective systems produce the greatest number. During the winter months the largest contributors to meteotsunamis are fronts and cyclones.

4.2.2: Case 2 Analysis

This case is unique in the fact that there was wind damage from this storm, but the wind speeds did not reach severe criteria. At the time leading up to the event wind speeds were between 5 and 15 knots, as seen in Fig 4.2.4, which also shows the steady increase in wind speeds from 1200 UTC until around 1500 UTC. At 1500 UTC there is a slight decrease in sustained wind speeds. Fig 4.2.4 shows the same trend in wind gusts, up until 1600 UTC where there is a sharp increase in the gust speed. The maximum wind gust speed reached 36.2 knots, which does not qualify for a severe threat.

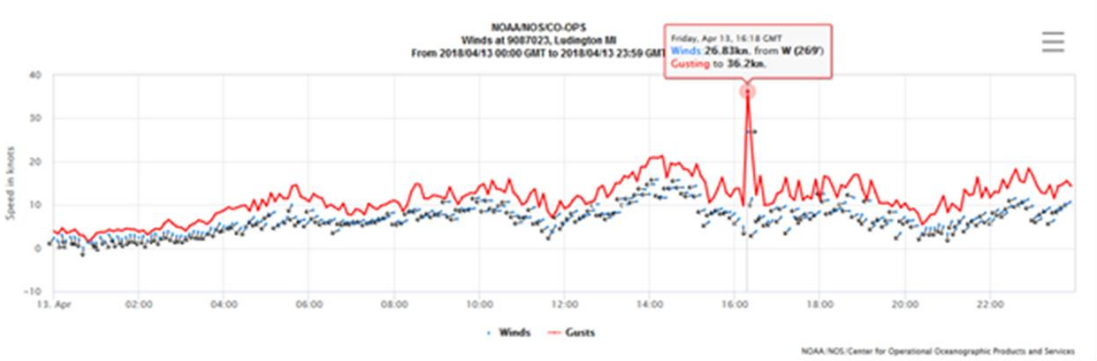

Figure 4.2.4: Time series plot of wind speeds and wind gusts valid for Ludington, Michigan, from 0000 to 2399 CST 13 April 2018. The red line represents the speed of wind gusts (in knots) and the blue dots represent wind speeds (in knots).

Another point to note was the shift in the sustained winds. Winds started out as easterly at 25 knots, then shifted to westerly at 35 knots. This resulted in a 60-knot vector change, likely contributing to the wind damage. This is significant because this wind shift occurred over a liquid surface, which caused objects such as docks and boats, to be pulled in once direction, then quickly thrown in the opposite direction. Boat damage and dock damage was reported from this storm.

An analysis of upper air charts was preformed to determine the location of the front as well as the conditions that contributed to the formation of the meteotsunami.

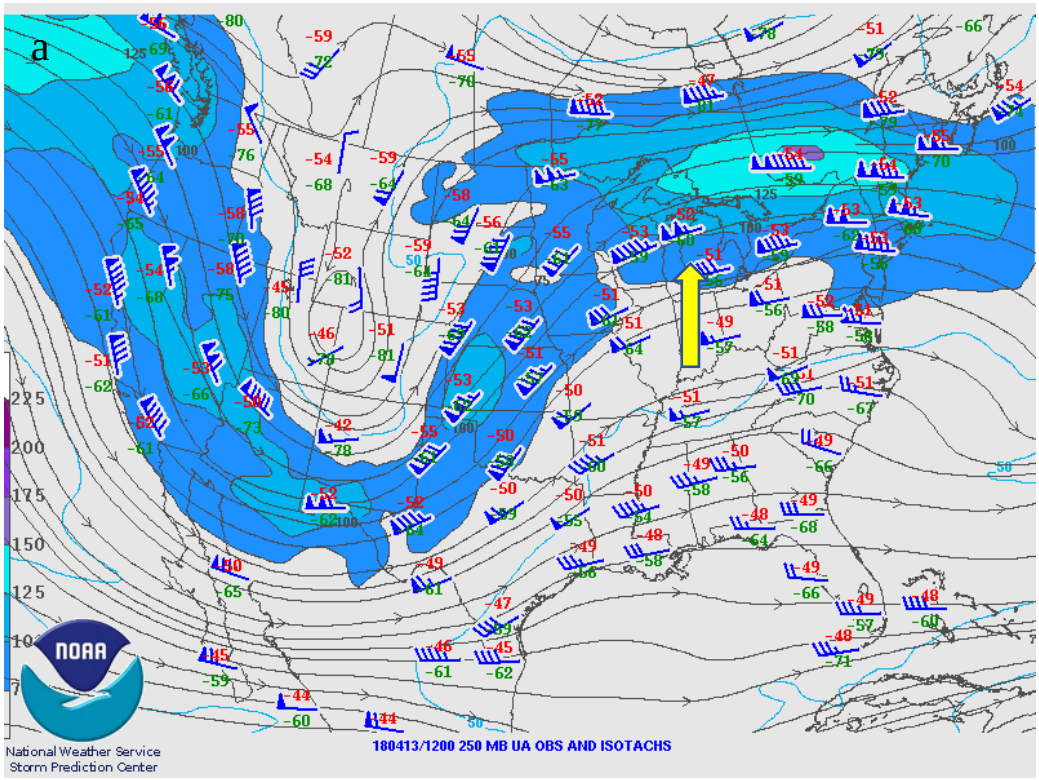

Figure 4.2.5: Upper-air analyses valid at 1200 UTC 13 April 2018 for a) 250-mb streamlines (solid black) and isotachs (solid blue, kt; shading > 75 kt); b) 500-mb geopotential height (solid black, dkm) and temperature (dashed red, deg C); c) 700-mb geopotential height (solid black, dkm), temperature (dashed blue/red, deg C), and dew point depression < 4 deg C (solid green); and d) 850-mb (dashed blue/red, deg C), and dew point depression < 4 deg C (solid green). Observations in standard station model format. The yellow arrow on each map points to the approximate location of Ludington, Michigan.

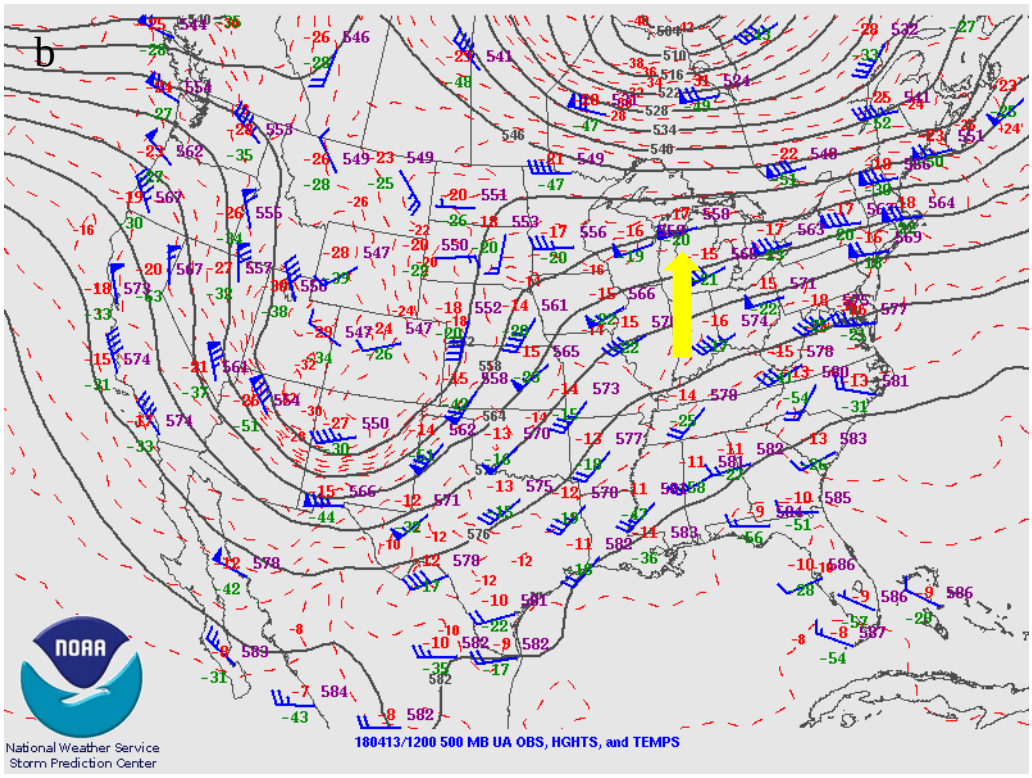

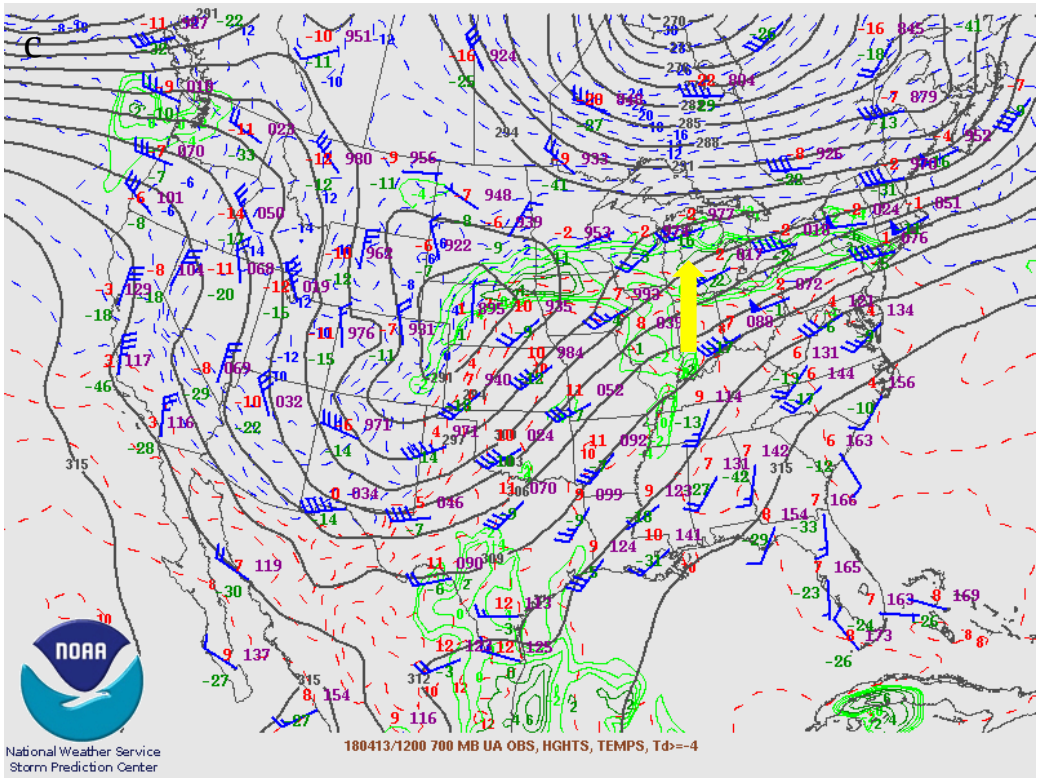

Figure 4.2.5: Continued.

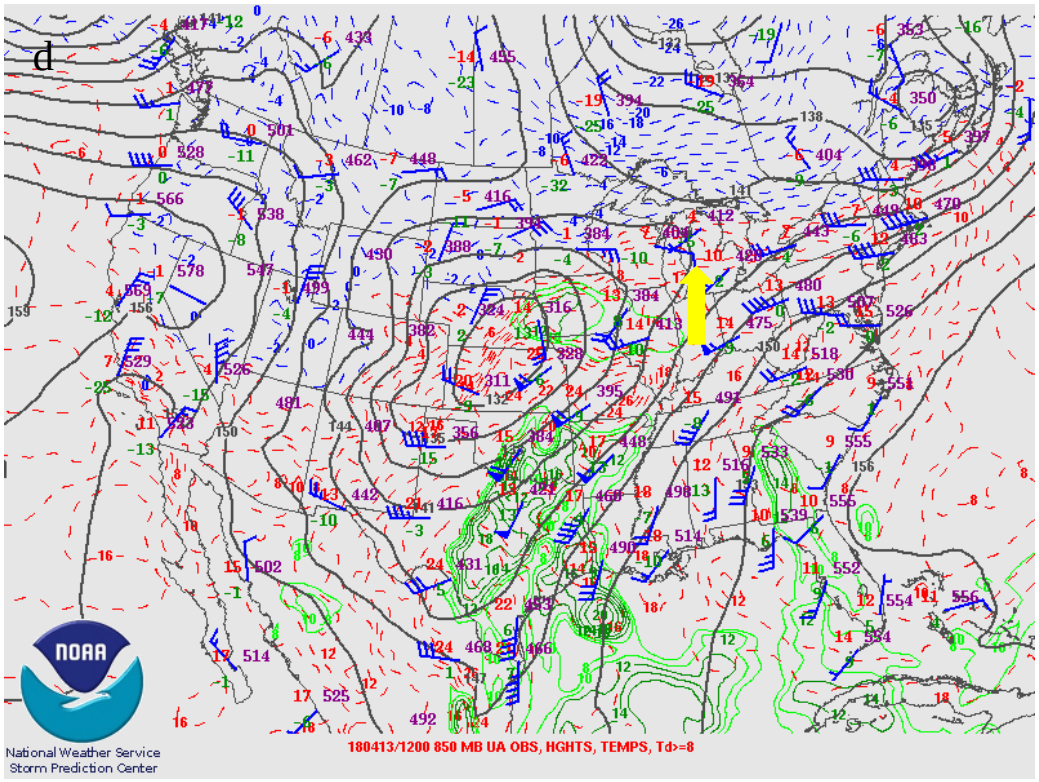

Figure 4.2.5: Continued

Figure 4.2.5a. shows a strong upper-level jet with speeds in excess of 90 kt over the area of interest. Also, Ludington is located in the right entrance region of the jet (on the downstream side of the trough) where divergence is maximized. Figure 4.2.5b. shows a deep 500-mb trough over the western continental U.S. Figure 4.2.5c shows the 700-mb low from the Four Corners region stretching up into Minnesota. As these charts are 4 hours before the time of the event, further verification was done using Plymouth State Weather Center (not shown) to confirm the location of the low at the time of interest, putting Michigan in the downstream flow of the low located in western Iowa and southern Wisconsin. Figure 4.2.5d shows the location of the 850-mb low. The low has four closed isobars and extends from the Central Plains to the Upper Midwest.

The surface analysis in Fig 4.2.6 shows that Michigan is between a cold front, associated with a low over Quebec to the north and a stationary front to the south.

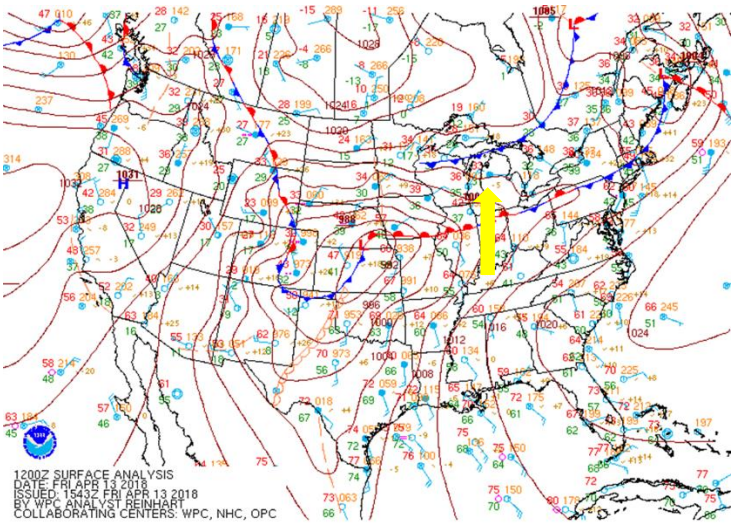

Figure 4.2.6: As in Fig. 4.1.2a, except valid at 1200 UTC 13 April 2018. The yellow arrow represents the approximate location of Ludington, Michigan.

The purpose in showing the upper air and surface charts is to determine that the convection the triggered the meteotsunami was caused by a frontal passage. This analysis determined that Ludington was in the downstream flow of the low and therefore the meteotsunami was influenced by the frontal passage.

As mentioned previously the water levels play a key role in the formation of meteotsunamis. At this time, Lake Michigan was experiencing record high water levels.

Figure 4.2.7: Time series plot of sea level pressure (mb) for Ludington, Michigan, valid 0000 to 2359 CST 13 April 2018.

These high-water levels in combination with changes in pressure are a large contributor to the formation of the meteotsunami. The pressure rose 10 mb in a matter of minutes shortly after 1600 UTC, as can be seen in Fig 4.2.7. This figure also shows a secondary pressure spike of approximately 5 mb after 1700 UTC. According to the gauges in Ludington, the water levels rose 1.51 feet at the time of the event. This led to some dock damage in Manistee, Michigan. Ludington-Sturgeon has the largest conditional occurrence percentage of meteotsunamis. This is due to the fact that is this one of the larger harbors on the Great Lakes. It has been shown that the larger the harbor the more favorable for energy transmission and amplification (Bechle et al. 2016).

The presence of gravity waves was suspected of contributing to the strength of the winds and the damage that occurred.

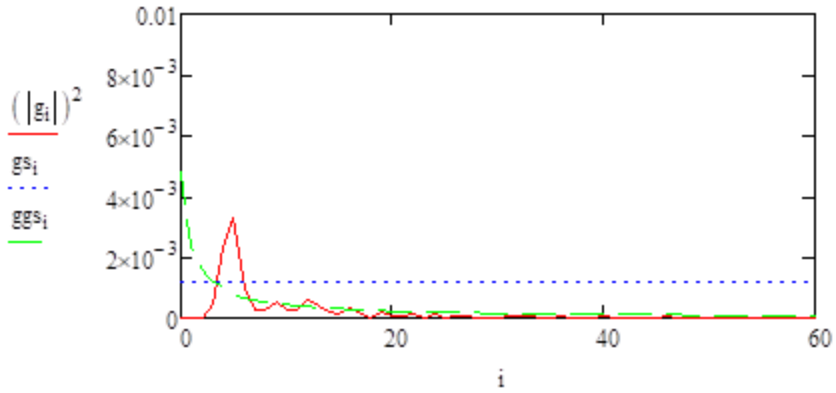

Figure 4.2.8: Fourier transform graph of 6 hours of 1-minute pressure data for Green Bay, WI on 13 April 2018 from 16 UTC- 22UTC. The x-axis is the wave number per 6 hours, and the y-axis is the surface pressure spectral power in inches squared. The blue dashed line represents the 95% confidence level. The red line is the blue noise for statistical significance and the green line is the red noise for statistical significance.

A Fourier transform was performed on one-minute pressure data (from Green Bay, Wisconsin) to determine the presence and frequency of such gravity waves. It was determined there was likely a gravity wave every hour (Fig 4.2.8) by the spike in the wave number around 6. These gravity waves were re-inforced by the elevated convection and there were three convective waves with this system. When gravity waves are in sync with the thunderstorm there may be more wind damage as the waves aid in the ability of the downdraft to penetrate the stable layer.

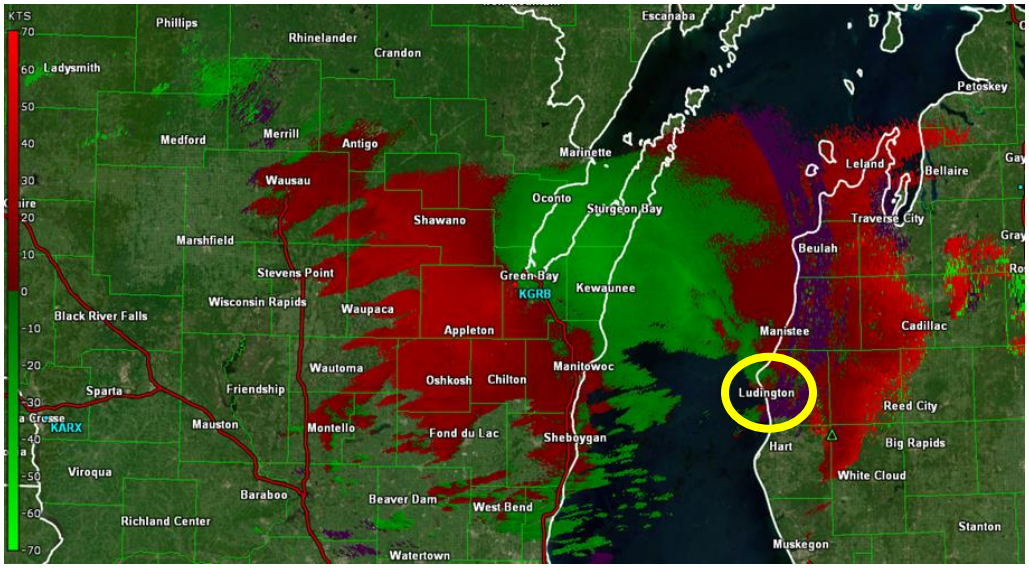

Figure 4.2.9: 0.5-degree base velocity radar image from Green Bay, Wisconsin (KGRB) valid at 1632 UTC 13 April 2018. Ludington, Michigan (the location of the pressure time series) is circled in yellow.

The analysis of the one-minute pressure data for Ludington, Michigan, was used to establish the presence of gravity waves, as they were not as clearly captured by radar. Fig 4.2.9 is the base velocity that shows a possible gravity wave between Manistee, Michigan, and Ludington, Michigan by the outbound velocities imbedded in the inbound velocities.

For the sounding portion of the analysis, soundings from two locations were chosen. Green Bay, Wisconsin, was chosen as the first location for the sounding analysis to determine the state of the atmosphere as the storm prepared to move across Lake Michigan. This site was also chosen due to the fact that the storm produced hail at this location and no severe wind reports were recorded as is seen in Fig 4.2.1. Multiple model soundings were examined, including experimental WRF wet and WRF dry (provided by Dr.

Greg Mann), as well as operational RAP and HRRR. There were minimal differences between these model solutions, so the RAP model soundings were used in this case for the sake of consistency.

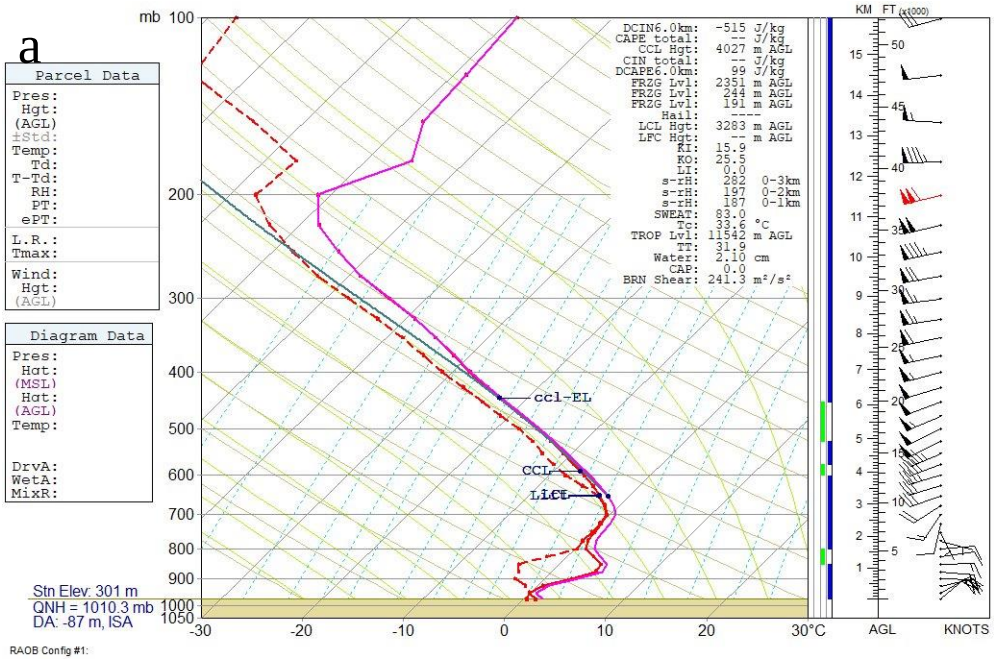

Figure 4.2.10: RAP model soundings for Green Bay Wisconsin, valid for 13 April 2018 a)1400 UTC, b)1500 UTC, c)1600 UTC, d) 1700 UTC.

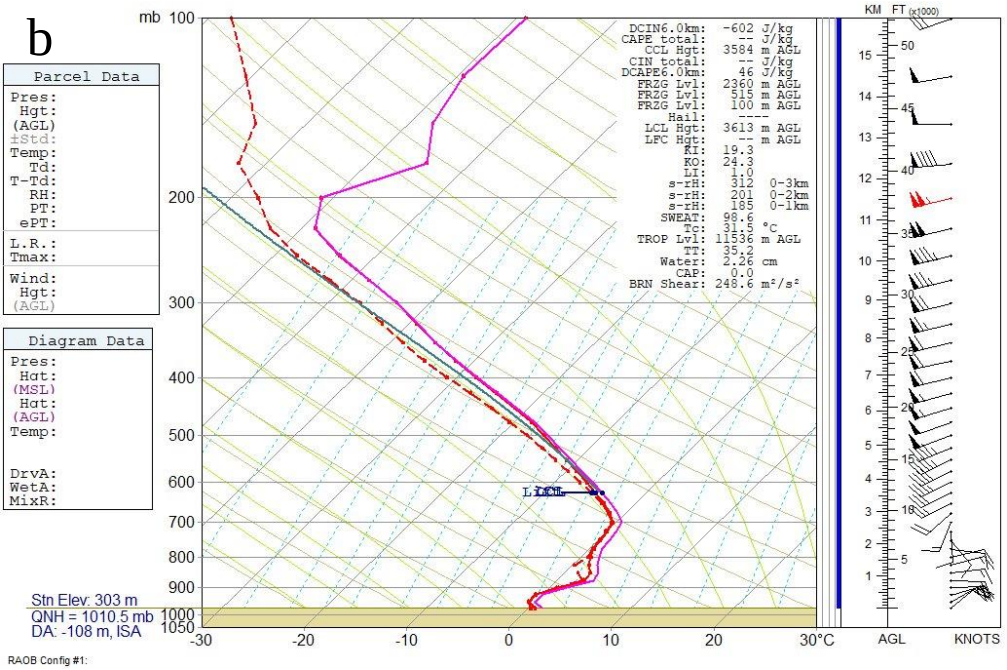

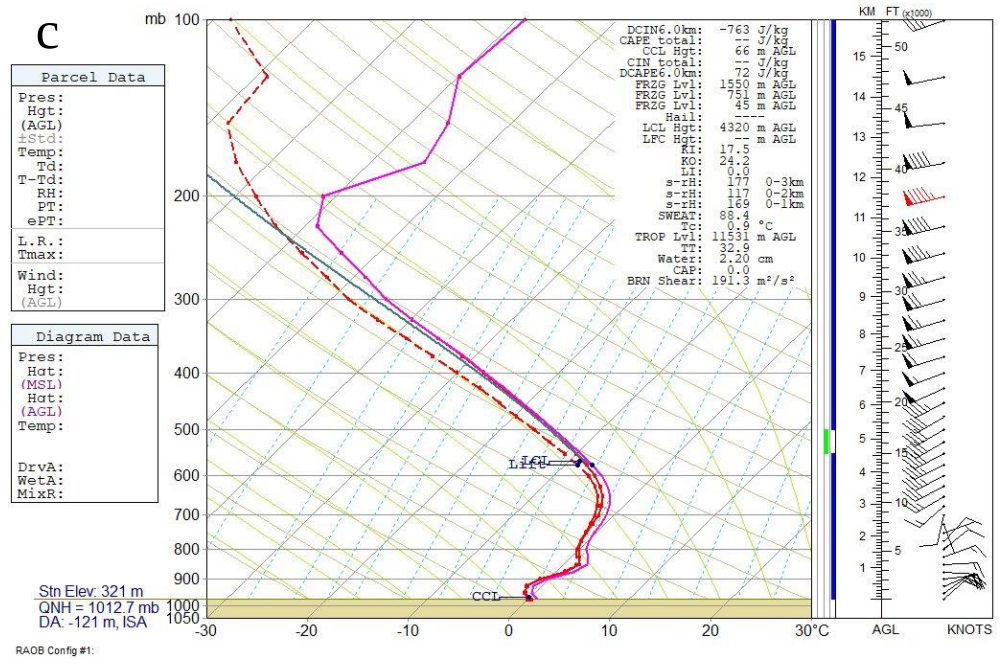

Figure 4.2.10: Continued

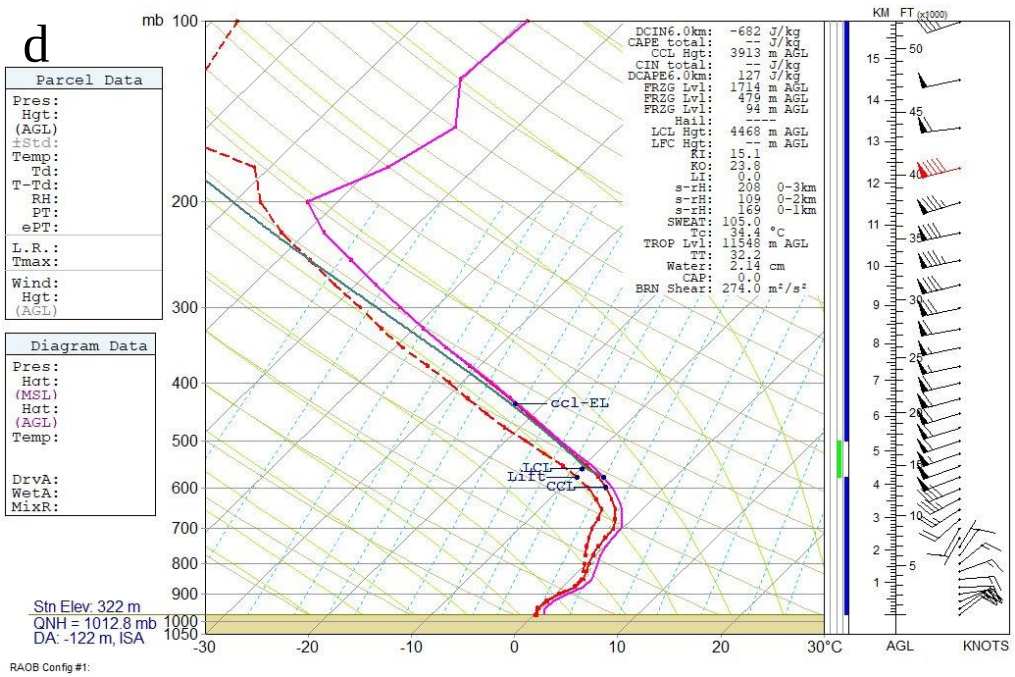

Figure 4.2.10: Continued.

Four soundings were used to determine the pattern of DCIN and DCAPE. As previously mentioned, the main threat from the system at this location was hail, and these soundings support that, as well as the hypothesis that a greater DCAPE is needed to produce severe wind at the surface. Fig 4.2.10a shows DCIN values of -515 J kg^{-1} with DCAPE values of 99 J kg^{-1}. This produced a |DCIN/DCAPE| ratio near one value so strong winds penetrating the stable layer was unlikely. This pattern is evident throughout the rest of the sounding series with Fig 4.2.10b showing values of DCIN at -602 J kg^{-1} and DCAPE 46 J kg^{-1}, Fig 2.4.10c with DCIN values of -763 J kg^{-1} and DCAPE 72 J kg^{-1}, and Fig 4.2.10d with DCIN at -682 J kg^{-1} and DCAPE at 127 J kg^{-1}. This figure shows that leading up to and during the time of the event in there is a steady increase in the values of DCIN while the DCAPE values remain fairly low.

This pattern supports the hail seen in Green Bay, Wisconsin, and the lack of severe wind reports. In Fig 4.2.10d there is a slight decrease in the value of DCIN while the DCAPE value increases; however, the DCIN is still much larger than the DCAPE and the ratio is still near 1, again with the ratio being the absolute value of DCIN over DCAPE. In fact, the DCIN was greater than the DCAPE by a factor of two throughout this time period.

The next set of soundings that was analyzed are from Ludington Michigan, where the wind damage was reported. The same time period was analyzed as the Green Bay soundings. In Fig 4.2.11a different pattern is seen between the values of DCIN and DCAPE. While DCIN is still the larger values, DCAPE has increased. In Fig 4.2.11a. the values of DCIN are -285 J kg^{-1} with DCAPE values of 267 J kg^{-1}. At 1400 UTC we see DCIN and DCAPE are nearly equal to each other. Fig 4.2.11b. shows values of DCIN at -309 J kg^{-1} and DCAPE at 257 J kg^{-1}. This shows that the DCIN values are slightly increasing while DCAPE remains fairly consistent. Figure 4.2.11c. (1600 UTC, the time of greatest interest) shows DCIN values of -399 J kg^{-1} and DCAPE at 202 J kg^{-1}. This shows the continual rise of the DCIN values while DCAPE decreases slightly. Finally, in Fig 4.2.11d. DCIN values are at -416 J kg^{-1} with DCAPE at 272 J kg^{-1}. At the location of greatest interest, Fig 4.2.11 shows that the values of DCIN and DCAPE were similar.

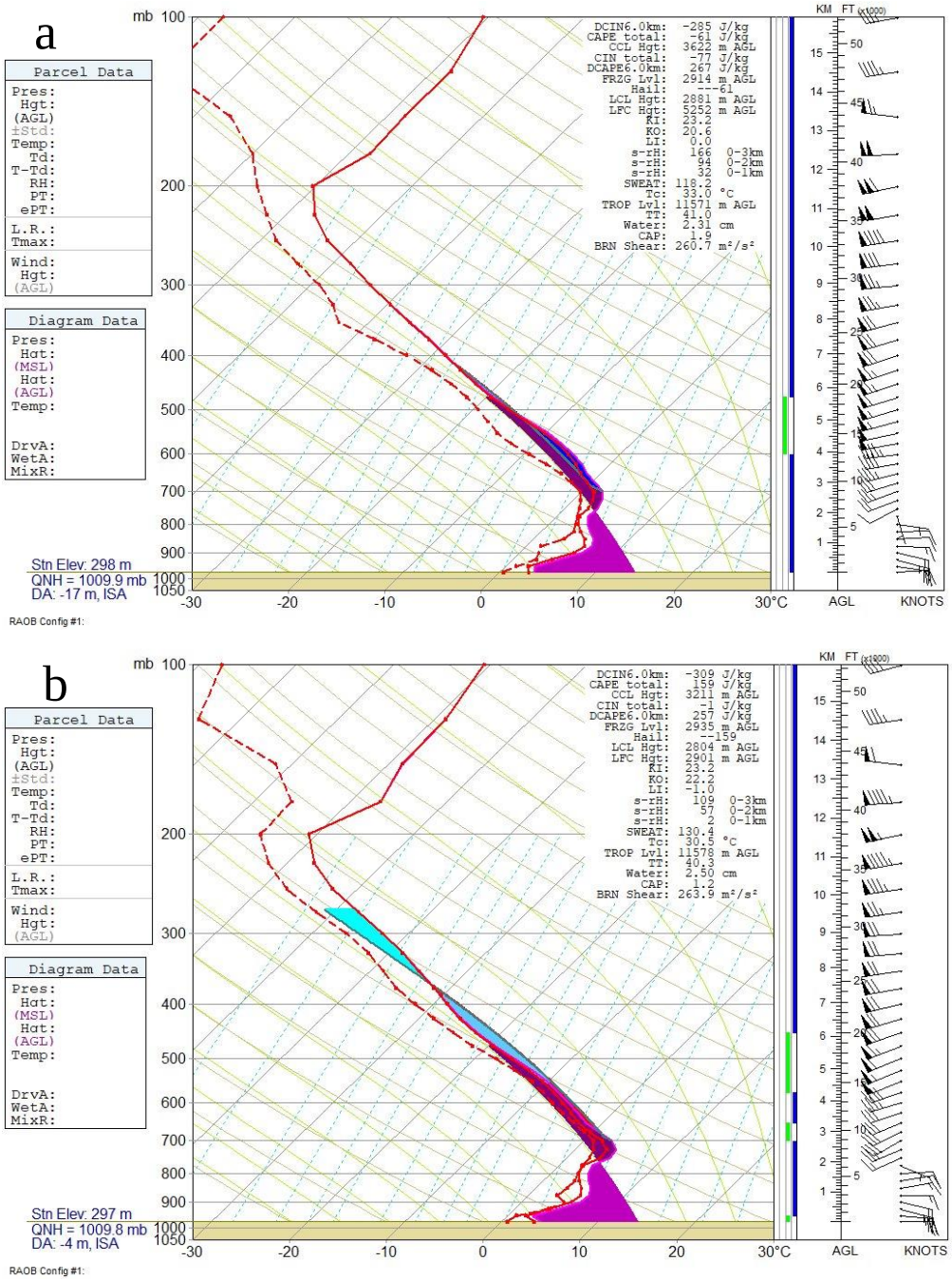

Figure 4.2.11: RAP model soundings for Ludington Michigan valid 13 April 2018 a) 1400 UTC, b) 1500 UTC, c) 1600 UTC, d) 1700 UTC. The dark purple shading represents the DCAPE and the light purple shading represents the DCIN.

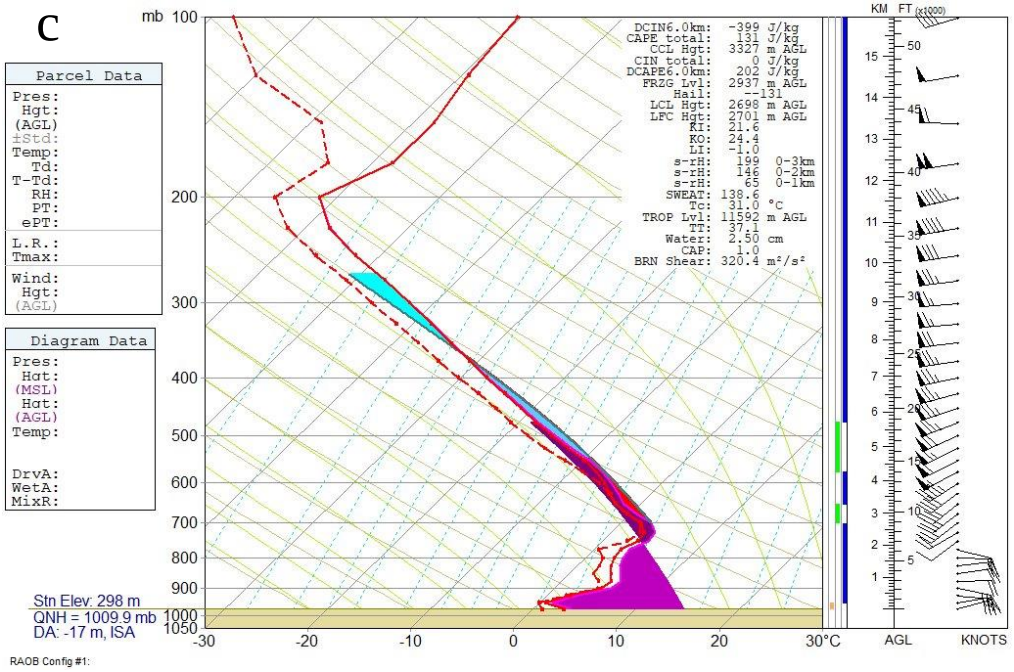

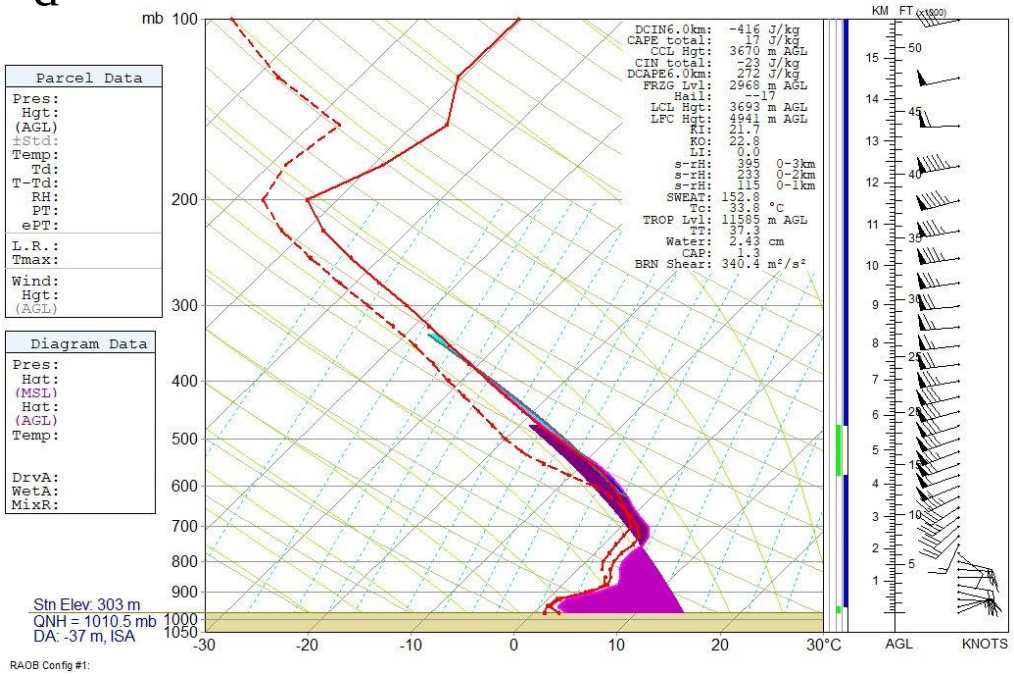

Figure 4.2.10: Continued

Values of DCIN and DCAPE being closer to each other would make it more possible for strong winds to penetrate the stable layer. However, this is not a

clear indication that severe winds at the surface will be experienced. Indeed, from Figure 4.2.1 it is clear that severe criteria winds did not reach the surface even though wind damage was observed.

4.2.3: Case 2 Summary

This case supports the hypothesis that severe winds will penetrate the stable layer when the |DCIN/DCAPE| ratio is near zero. In this case the ratio was closer to one than to zero. While some wind damage was observed, wind speeds did not reach severe criteria level. In addition, it was shown that in the case of hail, DCIN was much greater (by a factor of 2) than the DCAPE. Also present in this case were gravity waves interacting with the elevated convection. This gravity wave presence likely aided in the damaging winds, as well as the meteotsunami, as it encouraged the downward transfer of momentum.

4.3: Case 3 Overview

Case 3 was chosen for its transition from a hail-dominant storm to wind-dominant. This is a common pattern that has been identified. Initially it was thought that the storms all started out as hail-dominant then switched to wind-dominant. However, this is not the case. Storms can start out as either hail-dominant or wind-dominant, then transition to the other one, or never have

dominance of either type. It is the goal of this case to discern a pattern in the values of DCIN and DCAPE as the transition occurs.

Case 3 was chosen to expand upon work done by Grempler (2018) and his analysis of elevated convection using DCIN and DCAPE. This case study features a mesoscale convective system that occurred 29 May 2011. This storm occurred over the upper Midwest, from Nebraska through northern Illinois. At the start of the storm, in eastern Nebraska and western Iowa, the storm was hail-dominant, as can be seen in Figure 4.3.1.

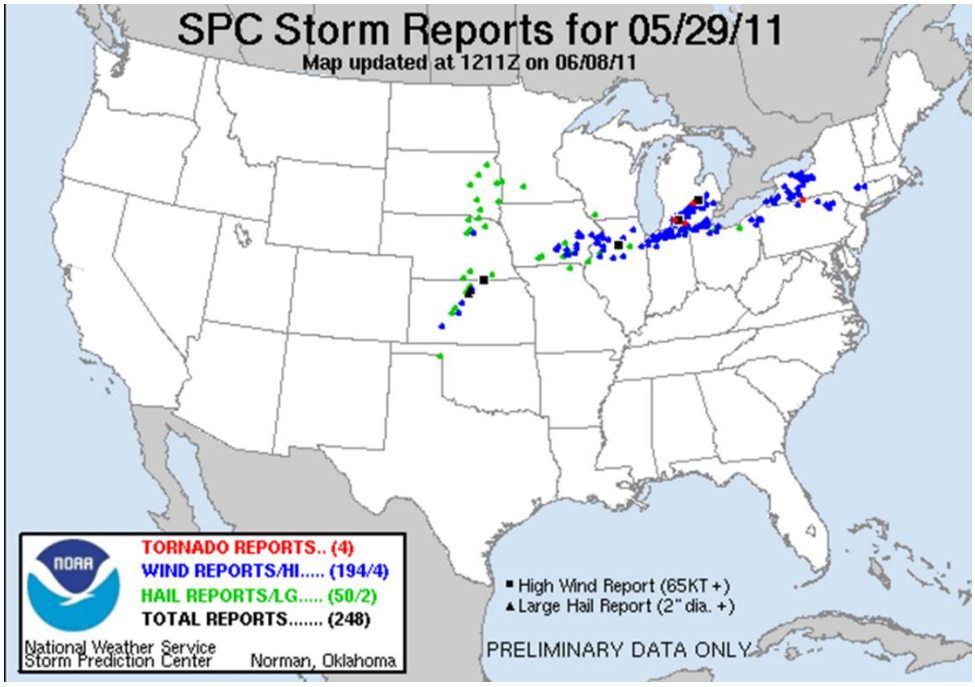

Figure 4.3.1: Storm reports from the Storm Prediction Center, valid for 29 May 2011. The blue dots represent wind reports. The green dots represent hail reports. The red dots represent tornado reports, and the black square represents a wind report of at least 65 kt.

The storm then transitions to being wind-dominant in central Iowa and remains that way through the duration of the storm. Also noteworthy is the mix of wind

and hail reports in northern Illinois. The first reports of severe weather occurred at 1121 UTC. The time frame that will be focused on in this case is from 1100 UTC, to capture the pre-convective environment, to 1800 UTC. A radar analysis as well as sounding analysis was used in this case. To track the progression of the storm as well as to identify trends in the DCIN and DCAPE values, four locations were chosen for analysis. The first location used was Omaha, Nebraska, at the start of the storm. The second location is Des Moines, Iowa. The third is Quad Cities, Iowa. The final location for analysis is Chicago, Illinois.

4.3.1: Case 3 Analysis

An analysis of upper-air and surface charts was done to determine the environment of the storm. Fig 4.3.1a shows a jet streak at the 300-mb level, which shows that the area of interest is located in the right entrance region providing the upper level support needed as it is in the preferred location for divergence. A strong trough is present over the Pacific Northwest at the 500-mb level Fig 4.3.2 b putting the area of concern in strong southwesterly flow. At the 850-mb level Fig 4.3.2. c shows the presence of a low-level jet with strong south-southwesterly flow that contributes significant moisture to the system. Finally, Fig 4.3.2.d shows a low-pressure system located in southwest Kansas, where a warm front stretches from Kansas through northern Missouri and into Illinois. Another feature to note in the surface analysis is the presence of easterly winds in Nebraska and southern Iowa.

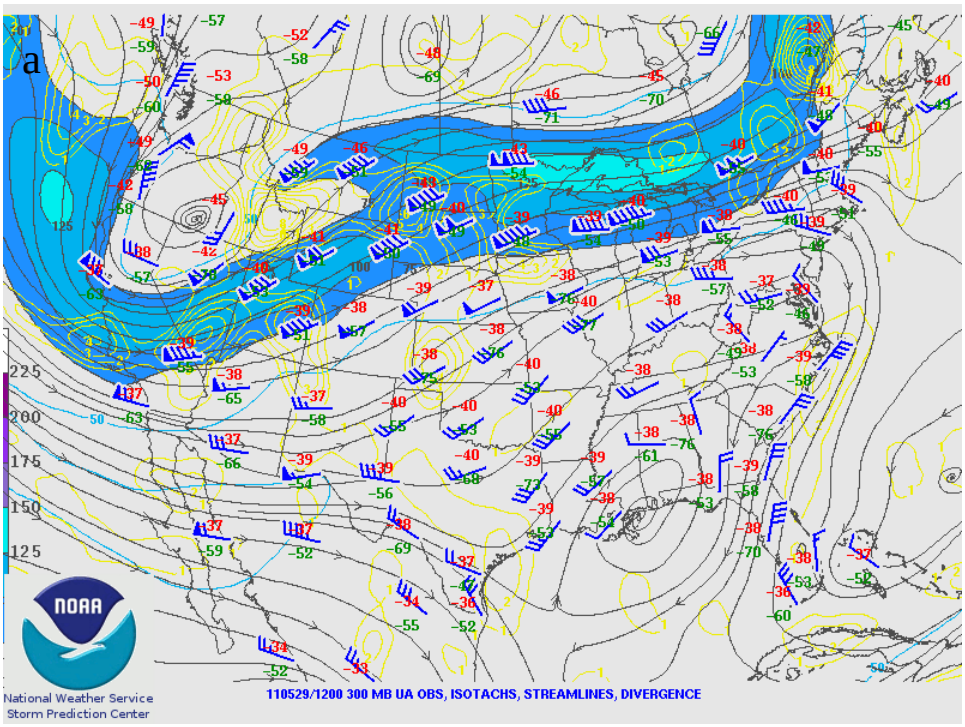
a
National Weather Service
Storm Prediction Center
110529/1200 300 MB UA OBS, ISOTACHS, STREAMLINES, DIVERGENCE

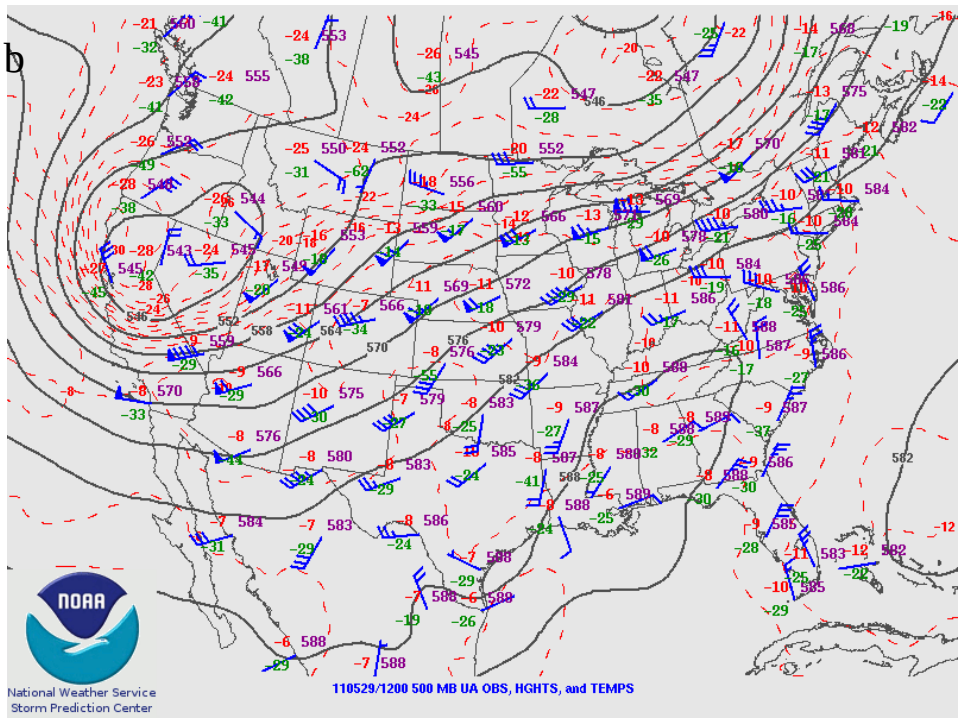
b
National Weather Service
Storm Prediction Center
110529/1200 500 MB UA OBS, HGHTS, and TEMPS

Figure 4.3.2: Valid for 29 May 2011 at 1200 UTC: a) 300-hPa isotachs, streamlines, and divergence (top left), b) 500-hPa observations, heights, and temperatures (top right), c) 850-hPa observations, heights (black-solid lines), temperatures (red-dotted lines), and moisture (green) (bottom left), d) Surface analysis (bottom right). Reproduced from the Storm Prediction Center and Weather Prediction Center

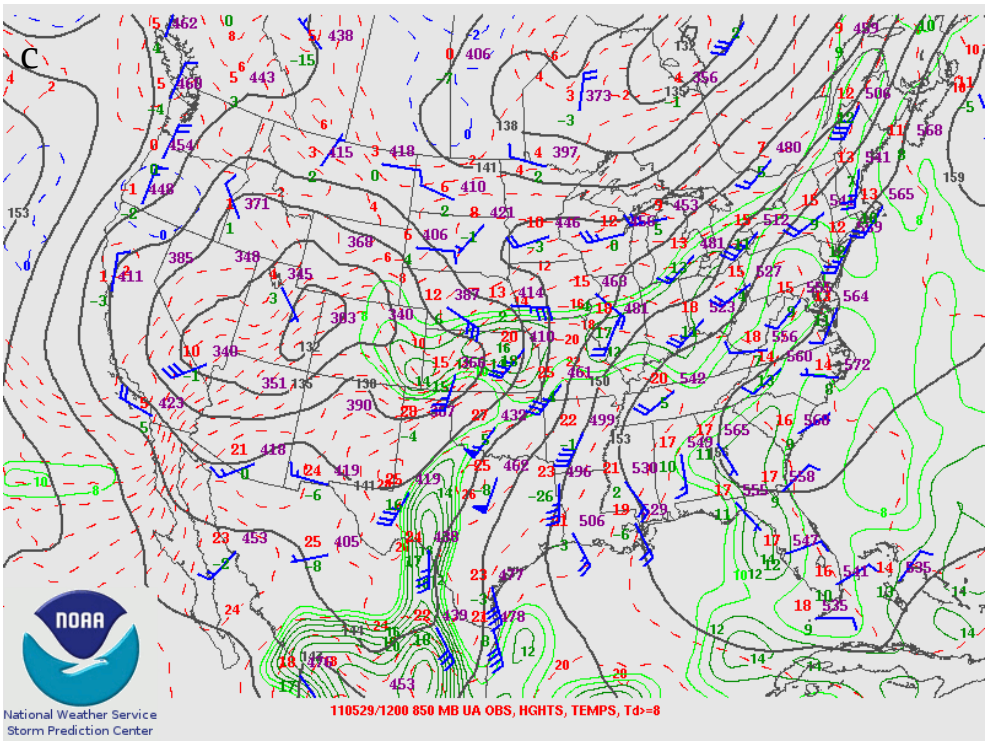

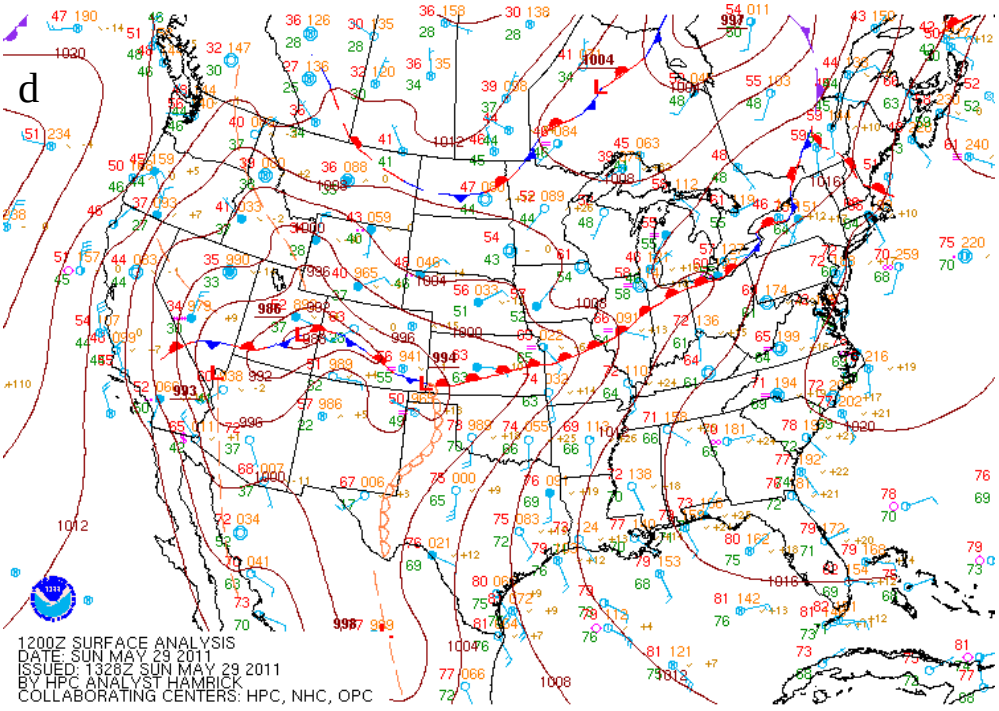

Figure 4.3.2. Continued

This first location chosen for analysis was Omaha, Nebraska. As previously mentioned, the first severe reports occurred at 1121 UTC 29 May 2011. Soundings were analyzed from 1100 UTC to 1800 UTC to discern any correlation between the |DCIN/DCAPE| ratio and the severe weather experienced. Fig 4.3.3 shows four soundings for Omaha. The first sounding Fig 4.3.3a. is valid at 1100 UTC, just before the first severe reports. This sounding shows values for both CIN and DCIN being 0, while DCAPE is 686 J kg^{-1} and CAPE is large at 1061 J kg^{-1}.

a

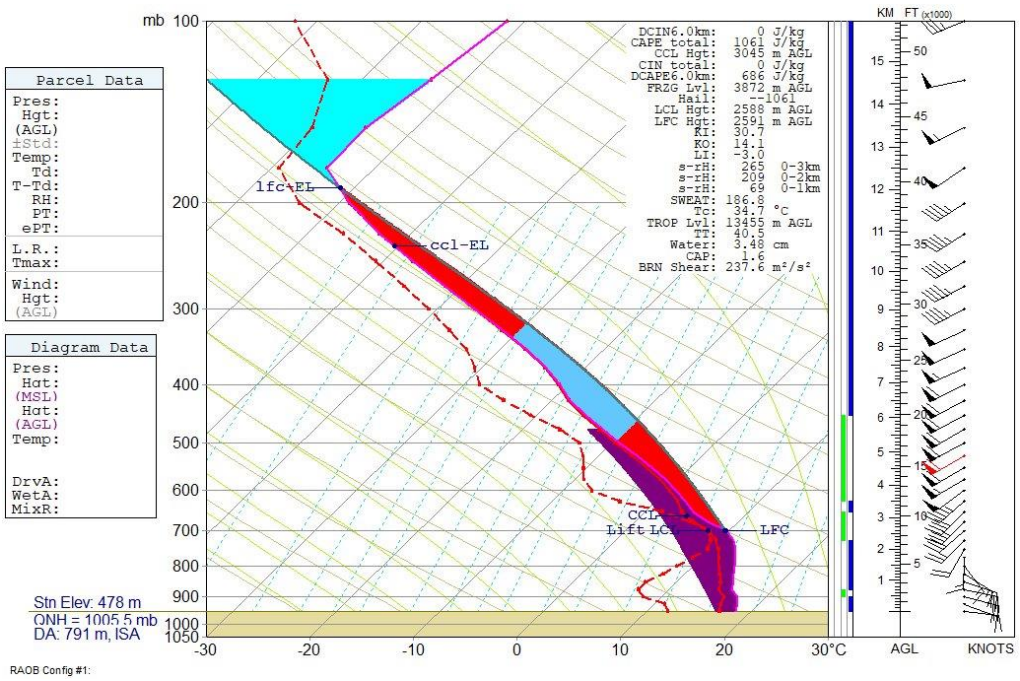

Figure 4.3.3: RUC soundings for Omaha, Nebraska valid for 29 May 2011 a) 1100 UTC, b) 1200 UTC, c) 1300 UTC, d) 1400 UTC. The dark purple shading represents the DCAPE and the light purple represents the DCIN.

b

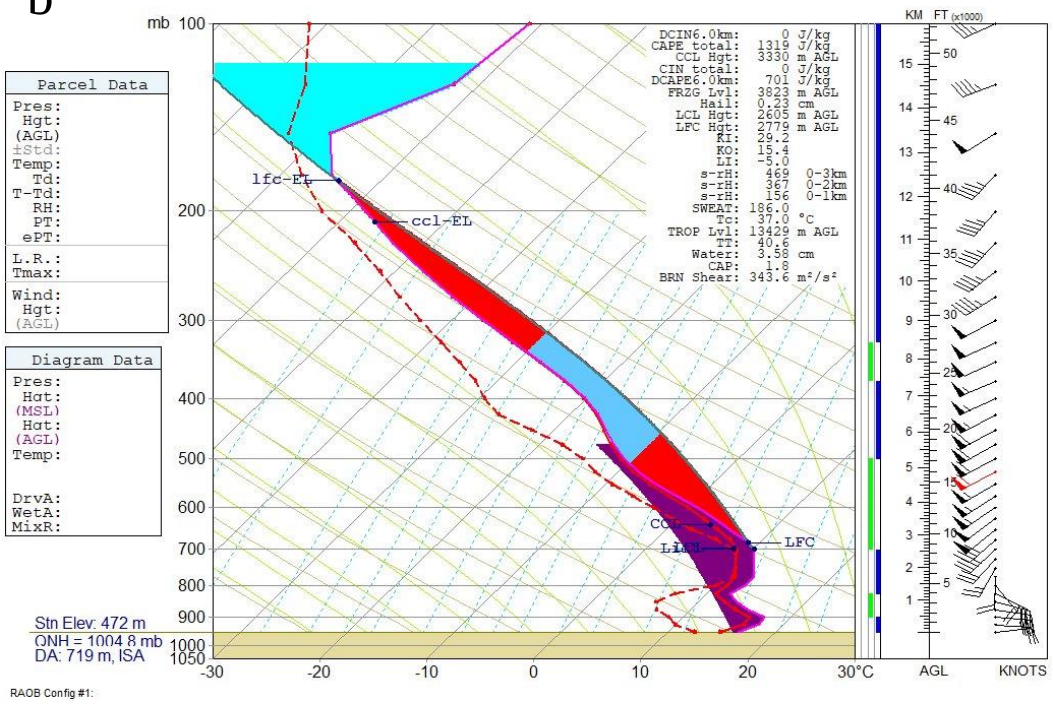

c

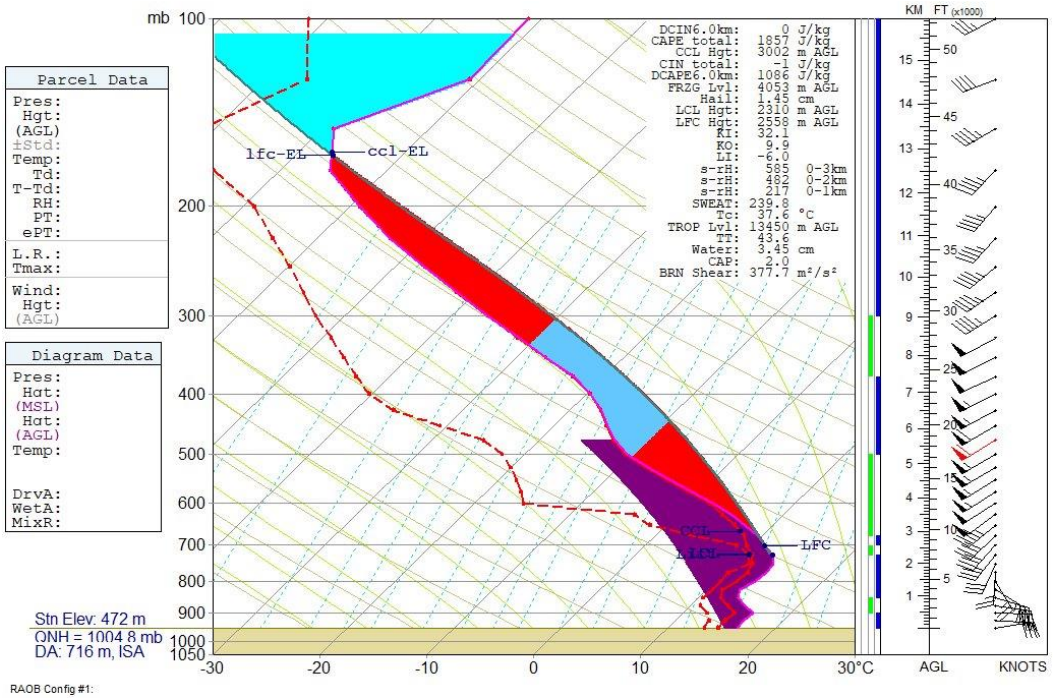

Figure 4.3.3: Continued.

d

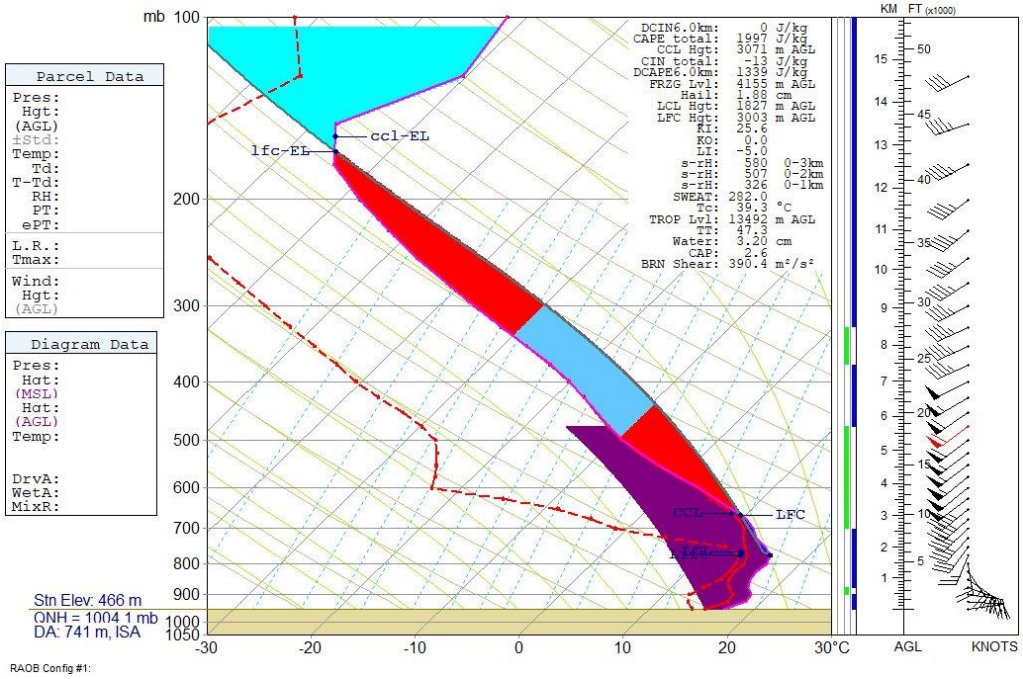

Figure 4.3.3: Continued

Fig 4.3.3b is similar to figure a in that the CIN and DCIN values are again 0 j kg^{-1}, while DCAPE is 701 J kg^{-1} and CAPE is 1319 J kg^{-1}. This shows a steady increase in both the DCAPE and CAPE values while DCIN and CIN remain non-existent. The 1300 UTC sounding (Fig 4.3.3c) again shows negligible values for DCIN and CIN while DCAPE and CAPE continue to increase with values of 1086 J kg^{-1} and 1857 J kg^{-1}, respectively. The final sounding (1400 UTC, fig 4.3.3d) shows that DCIN remains at 0 while there is a slight increase in CIN at -13 J kg^{-1}. Also shown is the continual increase in DCAPE at 1339 J kg^{-1} and CAPE at 1997 J kg^{-1}.

According to the hypothesis, these values of DCIN and DCAPE and their ratio would indicate that severe winds could penetrate the stable layer and reach the surface. However, no severe wind reports were recorded at this location at this time.

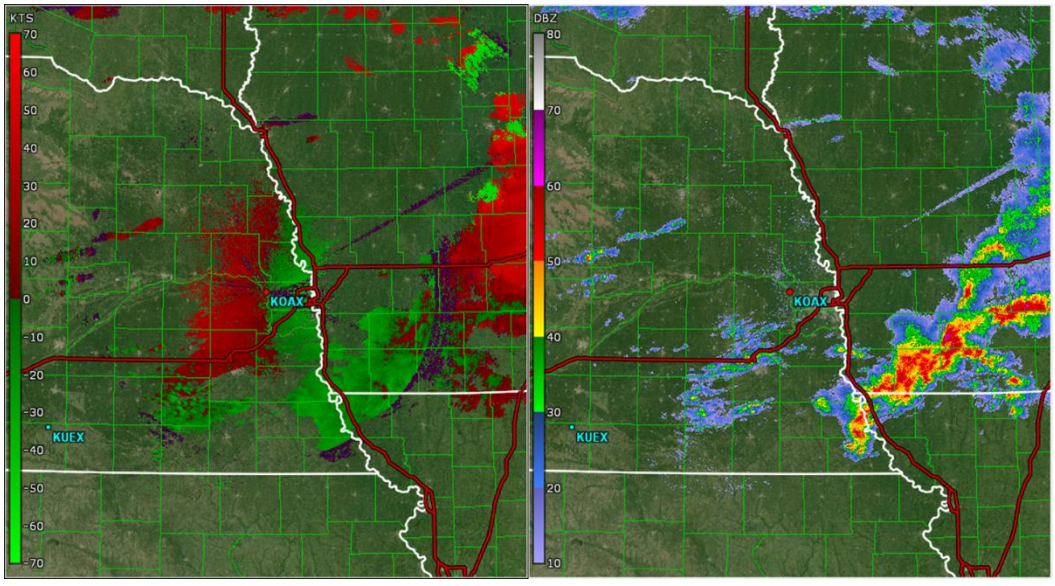

Figure 4.3.4: 0.5-degree base reflectivity (dBZ, left) and base velocity (kt, right) from the Omaha, Nebraska (OAX) WSR-88D valid at 1100 UTC 29 May 2011.

One explanation for the lack of severe wind reports even with the high DCAPE values can be seen in Fig 4.3.4, which shows the radar at 1100 UTC, the time of the first sounding analysis. It appears that the storm has already moved into northern Missouri and southern Iowa.

The next location of interest is Des Moines, Iowa. Again, four soundings were analyzed at the same times as the ones for Omaha.

a

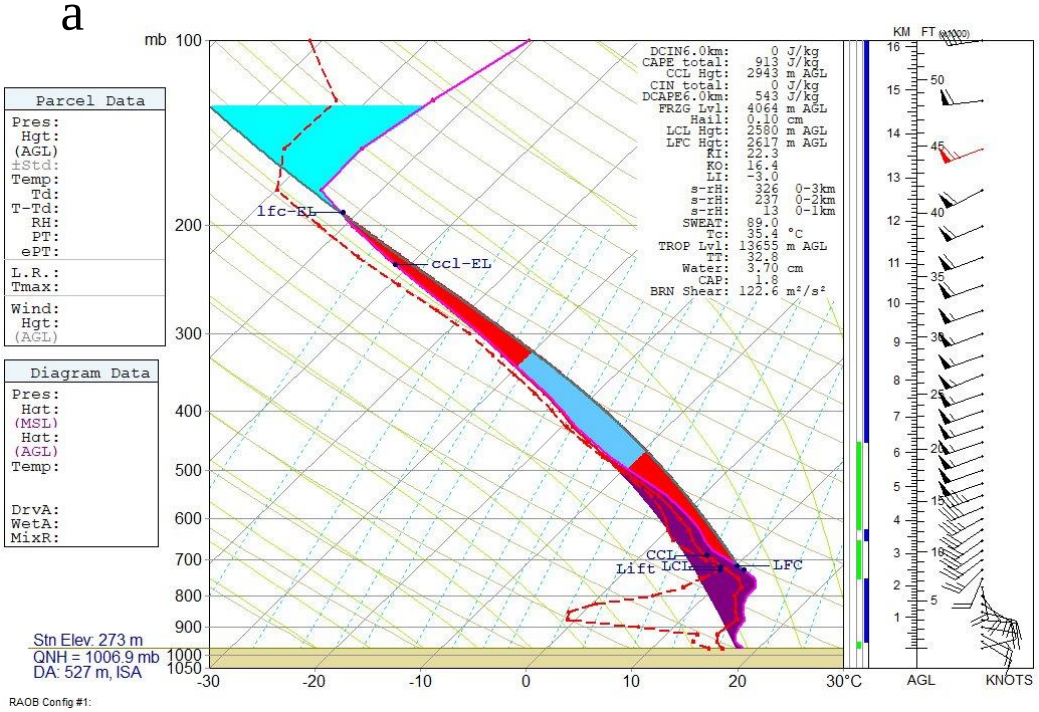

b

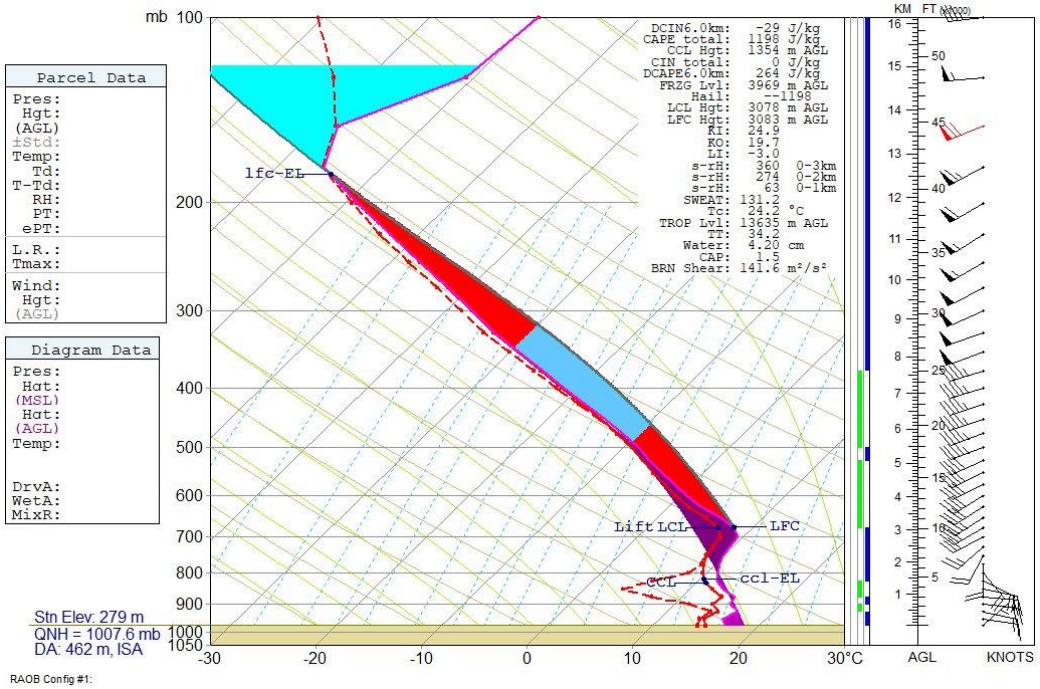

Figure 4.3.5: Soundings for Des Moines, Iowa, valid for 29 May 2011 a) 1100 UTC, b) 1200 UTC, c) 1300 UTC, d) 1400 UTC. The dark purple shading represents the DCAPE. The light purple shading represents the DCIN.

c

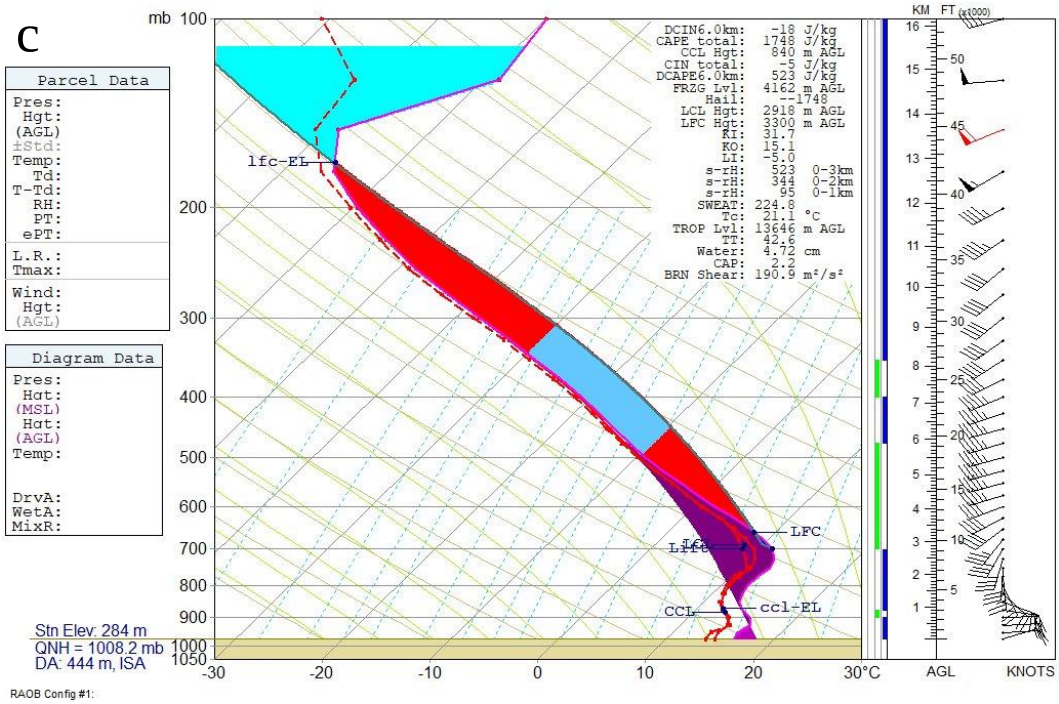

d

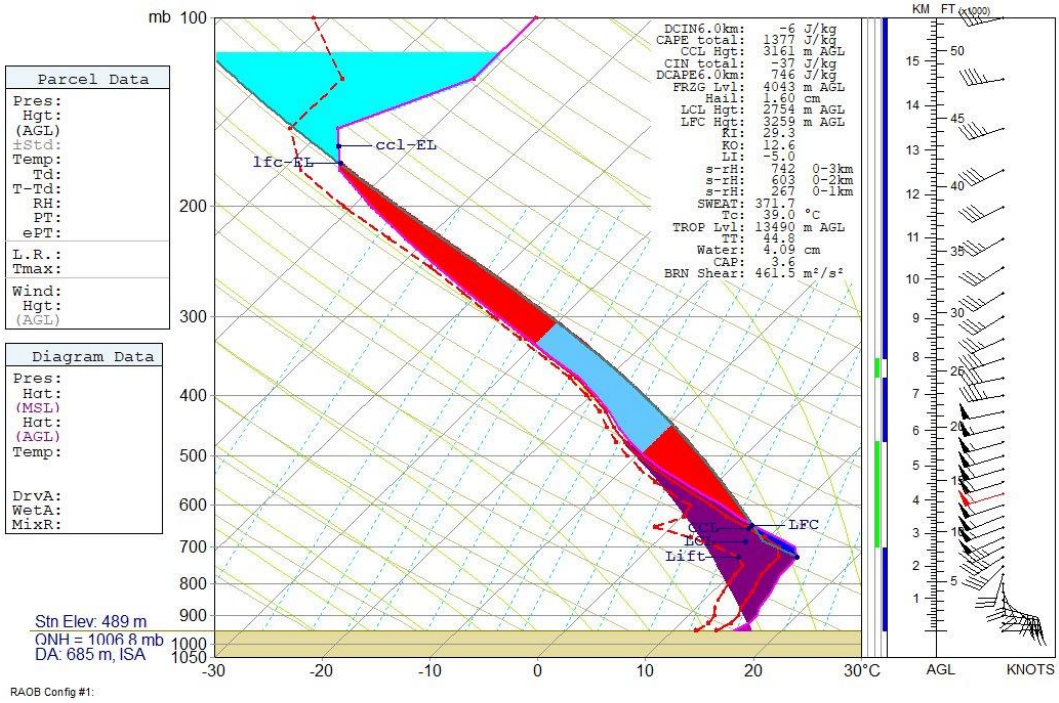

Figure 4.3.5: Continued

Fig 4.3.5a shows values of DCIN and CIN at 0 J kg^{-1}, much like the soundings for Omaha, and a DCAPE of 543 J kg^{-1} and CAPE of 913 J kg^{-1}. Fig 4.3.5b shows much of the same with DCIN and CIN at –29 J kg^{-1} and 0 J kg^{-1}, respectively, which is a slight increase in the DCIN but still negligible. The 1200 UTC DCAPE was 264 J kg^{-1}, while the CAPE at this time was 1198 J kg^{-1}

At this time, the DCAPE decreased by almost half while the CAPE continued to increase. By 1300 UTC (Fig 4.3.5c) the CAPE continued to increase (1748 J kg^{-1}) and DCAPE rebounded to 523 J kg^{-1}. The value of DCIN was again small at only -18 J kg^{-1} while CIN increased slightly (-5 J kg^{-1}). The 1400 UTC sounding (Fig 4.3.5d) showed a slight decrease in the CAPE to 1377 J kg^{-1} while the DCAPE value increased to 746 J kg^{-1}. At this time, there are nonzero values for both CIN and DCIN but again they remained low at -37 J kg^{-1} and -6

J kg^{-1}, respectively. Once again, the values of DCIN and DCAPE would indicate that severe winds were possible. When looking at Fig 4.3.1, it can be seen that there were severe wind reports around Des Moines. Other soundings (not shown) were analyzed to look for a continual pattern as the storm progressed. The common trend identified was that both CAPE and DCAPE values continued to increase with CAPE reaching a maximum over 3000 J kg^{-1} around 1700 UTC. DCAPE was maximized (1600 J kg^{-1}) at the same time.

Radar imagery were also analyzed for this case to determine the presence or absence of gravity waves, as well as to provide a visual reference for the movement and evolution of the storm. As with the first two cases a hypothesis was formed that gravity waves interacted with elevated convection and intensified winds at the surface.

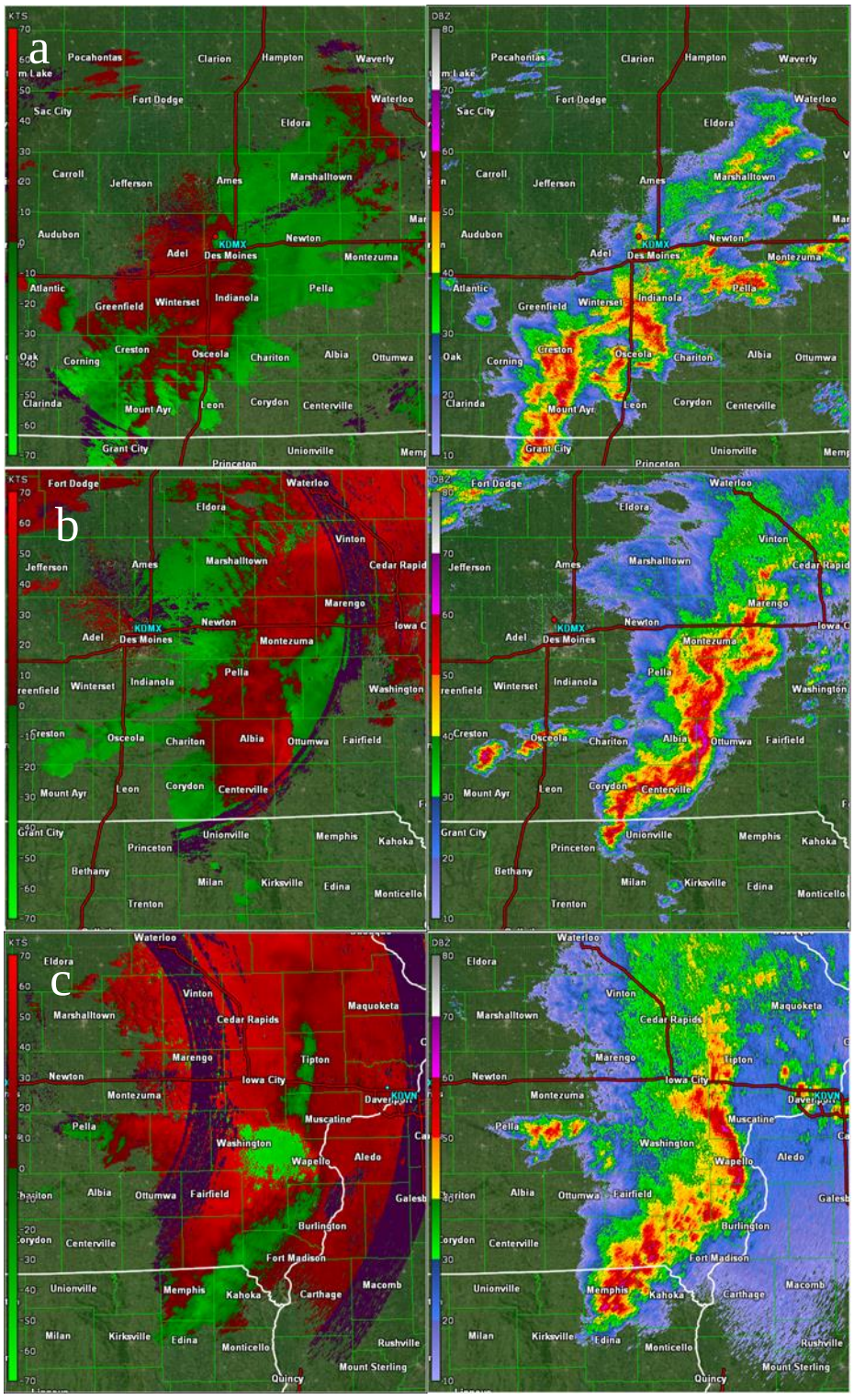

Figure 4.3.6: 0.5-degree base reflectivity (dBZ, left) and base velocity (kt, right) for Des Moines, Iowa, (KDMX). WSR-88D valid 29 May 2011 a) 1203 UTC, b) 1339 UTC, c) 1458 UTC.

Fig 4.3.6 shows some interesting activity on the radar in both base velocity and base reflectivity. Looking at the reflectivity in Fig 4.3.6a the storm is becoming more organized. At 1339 UTC (Fig. 4.3.6b) base reflectivity shows the storm is beginning to bow out, which would indicate the increased likeliness of strong winds at the surface. The last noteworthy feature is shown in Fig 4.3.6c in the base velocities. There is an interesting pattern of incoming and outgoing winds embedded around each other, around Washington, Iowa, which could contribute to strong winds. The structure of the storm as it starts to bow out, paired with the high DCAPE values would suggest that his storm is capable of producing severe wind at the surface.

The next location for analysis is Quad Cities, Iowa. This location was chosen as it follows the path of the storm. The sounding analysis includes four soundings at later times than the previous two locations. The time frame of interest for this location is 1500 UTC through 1800 UTC. Fig 4.3.7a showed a similar pattern in the values of all parameters with one distinct difference: significantly lower values of CAPE (414 J kg^{-1}). DCAPE values are 397 J kg^{-1}, almost equal to the CAPE. DCIN and CIN are again low at -4 J kg^{-1} and -11 J kg^{-1}. At 1600 UTC the CAPE values increased to 603 J kg^{-1} while DCAPE remained fairly consistent at 389 J kg^{-1} (Fig 4.3.7b). Again, values of DCIN and CIN were low at -2 and 0 J kg^{-1} respectively. The 1700 UTC sounding is of particular interest because a large increase in CAPE occurred with values climbing to 1694 J kg^{-1}. DCAPE also showed a significant increase to 776 J kg^{-1} (Fig 4.3.7c). DCIN and CIN were virtually non-existent. The final figure

(4.3.7d) Showed a decrease in CAPE down to 1161 J kg^{-1} while DCAPE continued to increase to 974 J kg^{-1}. DCIN was still not present while CIN increased to -35 J kg^{-1}. The results from the sounding analysis for this location are similar to the previous locations in that there was a negligible amount of DCIN and CIN while DCAPE and CAPE dominated. DCAPE is present throughout the entire analysis, but rapidly increased after 1700 UTC. In addition to the CAPE, DCAPE, CIN and DCIN values, the soundings showed a slightly backing wind profile.

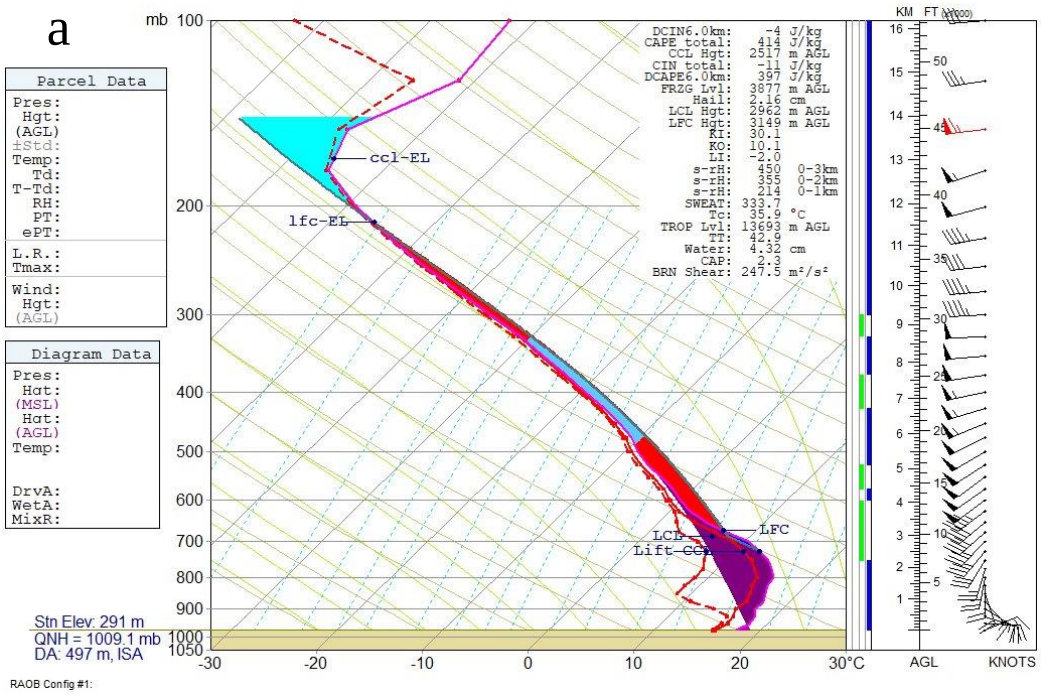

Figure 4.3.7: Soundings for Quad Cities, Iowa, (KDVN) valid for 29 May 2011 a) 1500 UTC, b) 1600 UTC, c) 1700 UTC, d) 1800 UTC. The dark purple shading represents DCAPE. The light purple shading represents DCIN.

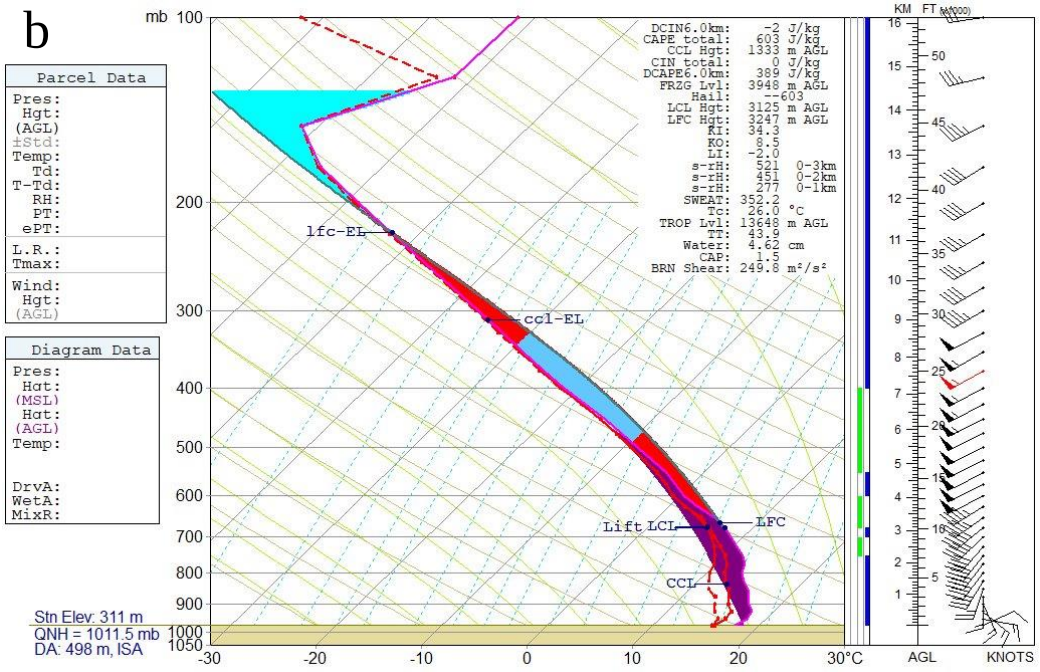

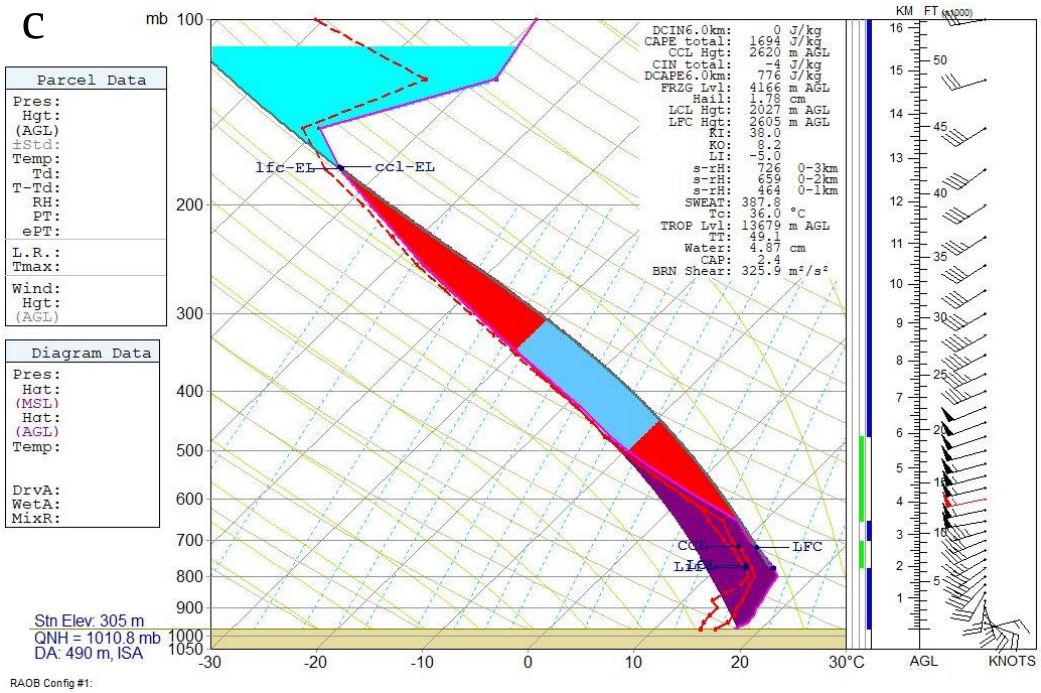

Figure 4.3.7: Continued

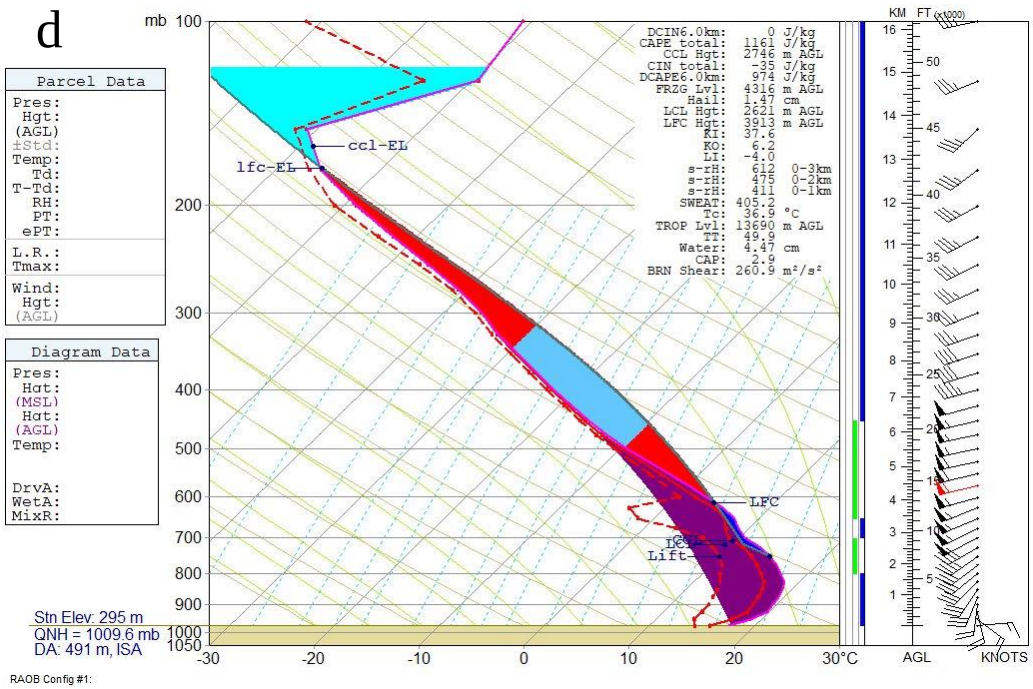

Figure 4.3.7: Continued

The final location chosen for analysis was Chicago, Illinois. Again, a series of four soundings are shown. The times chosen for this location's analysis are the same as the times for Quad Cities, 1500 UTC through 1800 UTC.

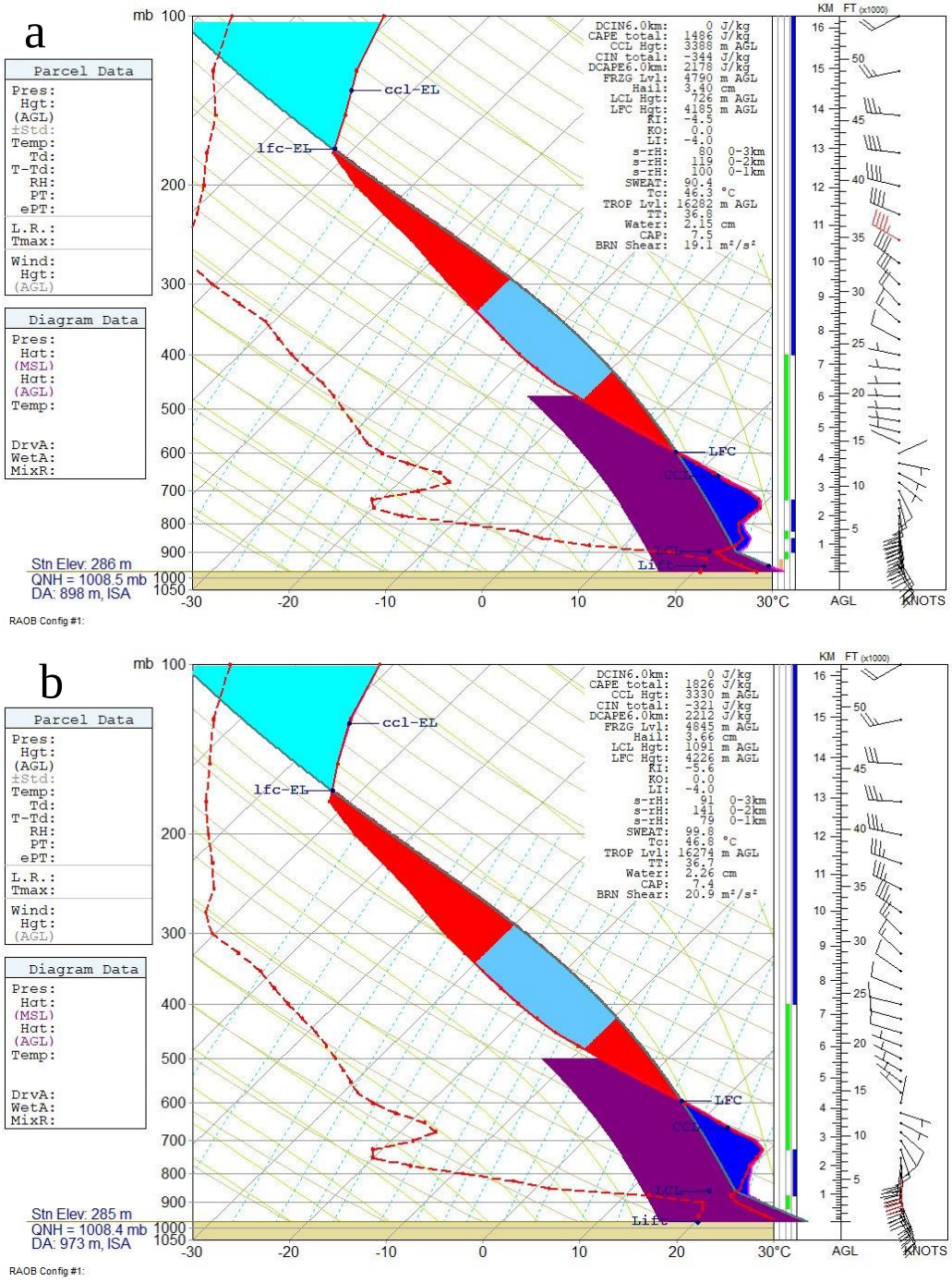

Figure 4.3.8: RUC model soundings for Chicago, Illinois, valid for 29 May 2011 a) 1500 UTC, b) 1600 UTC, c) 1700 UTC, d) 1800 UTC. The dark purple shading represents DCAPE. The light purple shading represents DCIN.

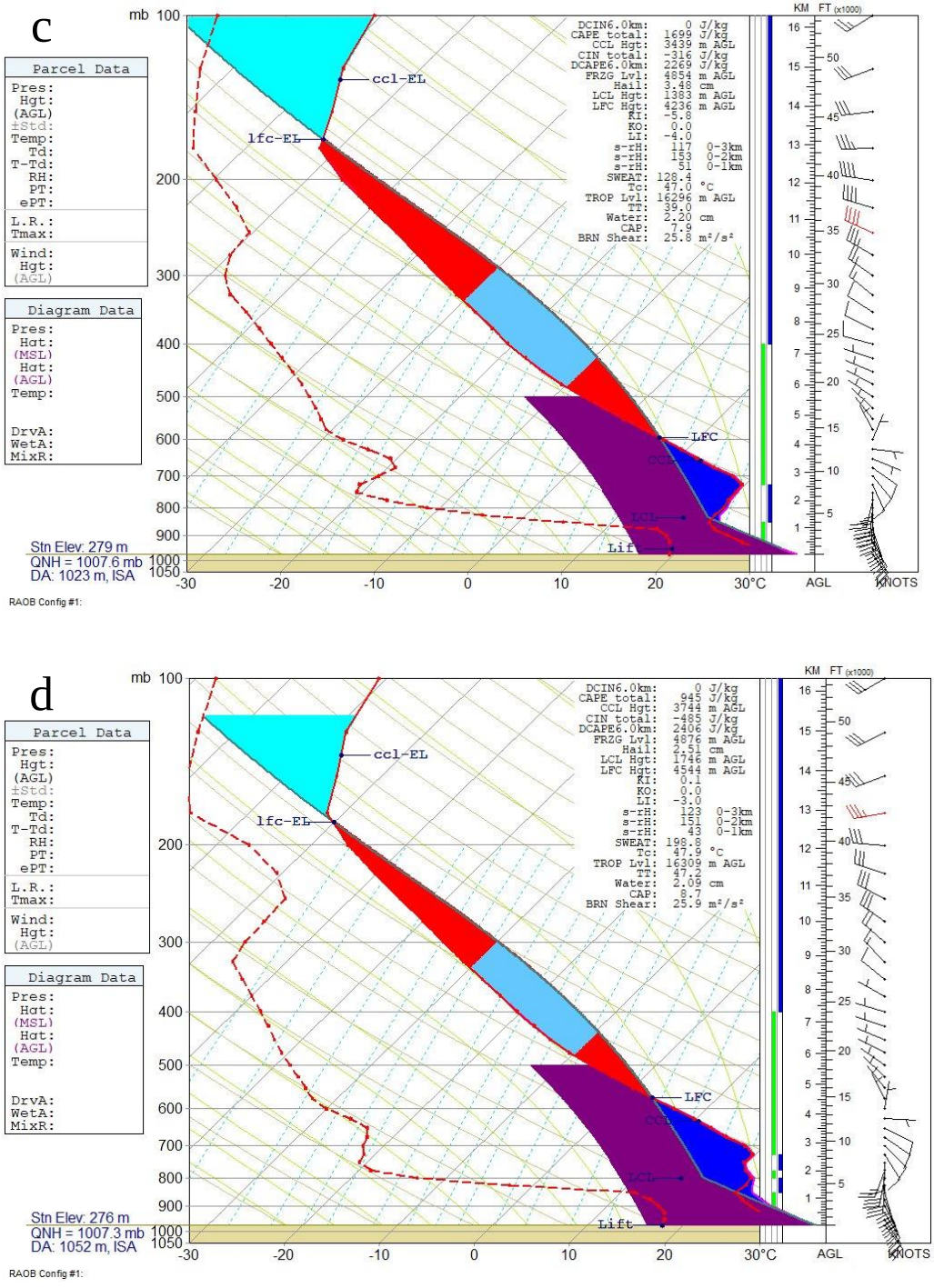

Figure 4.3.8: Continued

Figure 4.3.8 showed significantly large values of DCAPE present in all four soundings, illustrated by the dark purple shading. The 1500 UTC (Fig

4.3.8a) had values of DCAPE at 2178 J kg^{-1}, the largest values seen so far in the examination of this case. CAPE values were significantly less than DCAPE (1486 J kg^{-1}). One notable change in the 1500 UTC sounding (Fig 4.3.8.a) from all future soundings analyzed was an increased CIN value at -344 J kg^{-1}, while DCIN remains at 0 J kg^{-1}. The 1600 UTC sounding showed much of the same with DCAPE values of 2212 J kg^{-1}. CAPE values increased slightly to 1826 J kg^{-1} while CIN remained nearly the same at -321 J kg^{-1} and with 0 J kg^{-1} DCIN (Fig 4.3.8b). The 1700 UTC sounding was again similar to the other with DCAPE remaining fairly consistent with values of 2269 J kg^{-1}, CAPE values again slightly increasing to 1699 J kg^{-1}, CIN values of -316 J kg^{-1} and DCIN values remained at 0 J kg^{-1} (Fig 4.3.8c). The 1800 UTC sounding showed a decrease in the CAPE values to 945 J kg^{-1}. DCAPE increased slightly to 2406 J kg^{-1}. CIN values also increased slightly to -485 J kg^{-1}, while the value for DCIN remained 0 J kg^{-1}. Throughout this entire timeframe DCAPE remained large (over 2000 J kg-1), reaching a maximum value of 2400 J kg^{-1}. In addition, the temperature is significantly warmer in the lower levels than the previous locations. This warming could have contributed to the lack of severe hail reports, as the hail could have melted before reaching the surface.

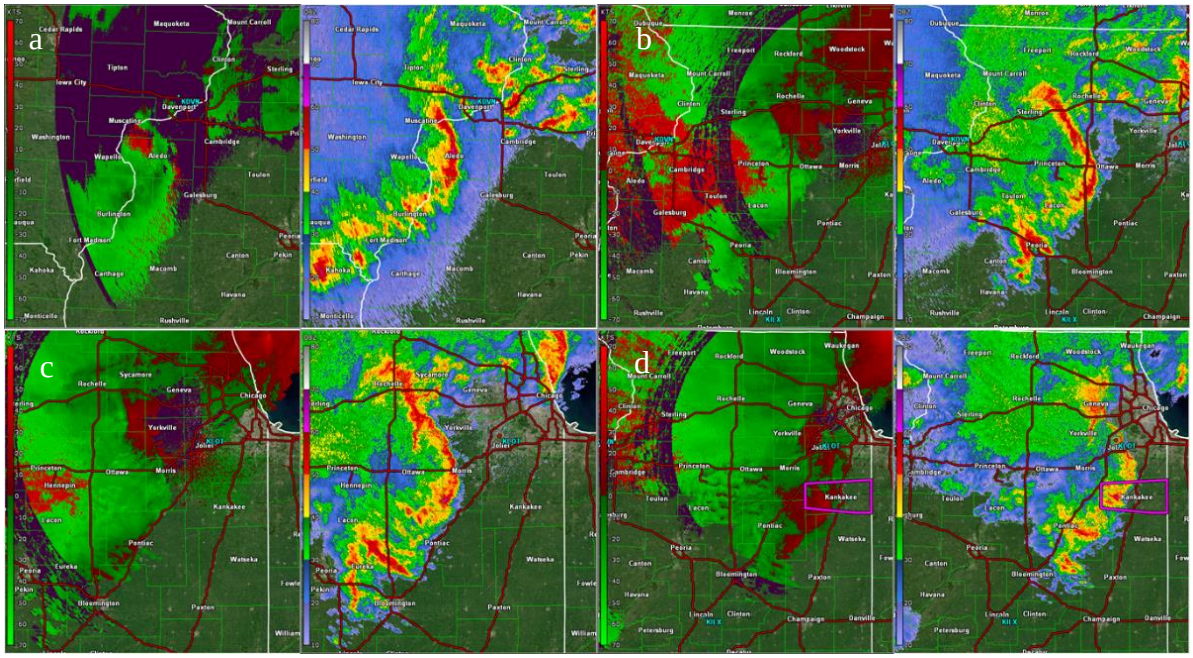

Figure 4.3.9: 0.5-degree base reflectivity (dBZ, left) and base velocity (kt, right) from Chicago, Illinois, (KLOT). WSR-88D valid 29 May 2011 a) 1521 UTC, b) 1656 UTC, c) 1723 UTC, d) 1756 UTC.

The radar analysis for Chicago also reveals some interesting characteristics of this storm. Again, a bowing out of the line can be seen in the base reflectivity images in Fig 4.3.9a. In Fig 4.3.9b the line became more organized and the bowing was more pronounced. The base velocity images in Fig 4.3.9 c. and d. showed gravity waves along the southern portion of the line by the inbound and outbound velocities once again embedded in each other. Fig 4.3.9. d. showed a tornado warning was issued for just south of Chicago.

4.3.2: Case 3 Summary

The purpose of case 3 was to discern an evident trend in the values of DCIN and DCAPE as a storm transitioned from hail-dominant to wind-dominant. The results were not what was expected. Although the values for

DCAPE remained high throughout the entire life of the storm at the positions analyzed and had a near zero value for DCIN, supporting strong winds reaching the surface, no recognizable pattern was found. One possible explanation for the behavior of this storm starting as hail-dominant and switching to wind-dominant is the diurnal influence. The majority of the hail was reported earlier in the day but as the day warmed fewer hail reports were obtained likely due to melting. The large CAPE values support hail and since the DCIN values were near zero throughout the entire period, the surface layer is not clearly assisting with hail survival. Another contributor to the large value for DCAPE is the dryness aloft that is evident in the soundings shown. The final thought as to why a recognizable pattern was not established between the form of severe weather and the |DCIN/DCAPE| ratio is the lack of a deep inversion with a significant layer of cooler air near the surface. A shallower inversion would likely aided in strong winds reaching the surface as the winds have a shallower stable layer to penetrate.

CHAPTER 5. CONCLUSIONS

5.1 Conclusions

The goal of this work is to contribute to the ongoing evolution of our understanding the DCIN and DCAPE parameters. Previous studies have used these parameters as a way to determine if convection was truly elevated, then as a way to predict flooding, and finally as a tool to predict potential severe weather from elevated convection. The aim of this research is to show that the |DCIN/DCAPE| ratio is a valuable forecasting and deterministic tool when it comes to predicting the type of severe threat a storm presents.

While only a limited number of cases were analyzed in this study, the results were promising. The first case provided a |DCIN/DCAPE| ratio near zero. Severe winds were experienced at the surface. In fact, this ratio was used in real time by NWS employees to assist with the decision to issue a severe thunderstorm warning. The second case also provided valuable results. The |DCIN/DCAPE| ratio was near 1, which would indicate it is less likely for severe winds to penetrate the stable layer and reach the surface. Even though wind damage was observed, the wind speeds (greatest speeds at 36 kts) never actually reached the severe criteria level. The final case in the study proved challenging. The goal was to determine a relationship between the

|DCIN/DCAPE| ratio and the dominant severe weather threat. While a clear relationship was not evident, the |DCIN/DCAPE| ratio of zero was present where severe winds were reported.

Analysis of gravity wave presence was compelling but not conclusive. The Fourier Transform of the one-minute pressure data that was performed for case 1 did not show clear gravity wave or oscillation patterns. While the pressure data was less than conclusive, gravity wavelike features were captured on the radar and calculations from that observed data were done to determine there was a gravity wave approximately every four minutes. The exact opposite occurred when analyzing gravity wave presence in case 2. No clear radar data was obtained to visually determine that gravity waves were present. The same Fourier Transform analysis of 1-minute pressure data was done for Ludington, Michigan. The pressure data for this location yielded better results and the presence of gravity waves and oscillations.

While none of this data is conclusive, it sets the groundwork for future studies on gravity waves interacting with elevated convection, and what role they might play in enhancing the likelihood of severe winds reaching the surface.

5.2: Future Work

The |DCIN/DCAPE| ratio is a valuable tool for forecasters. This research examined three cases, and applied the ratio, leading to encouraging results.

While this is a good start, there is much more work to do. Future work would include a more expansive pool of detailed case studies of elevated convective events to show the ratio can be applied, with success, anytime elevated convection is present. In addition to a larger case study pool being needed, more work on the evolution of storms that start out as hail-/wind-dominant then transition to wind-/hail-dominant is needed. The |DCIN/DCAPE| ratio would prove even more useful if it can be used to identify when the threat from a system will change from one type to another.

In addition, it would be valuable to determine how close to zero the DCIN/DCAPE ratio would need to be in order for the downdraft to penetrate the stable layer. It is unclear at this point how large the DCAPE in comparison to the DCIN needs to be for the downdraft to penetrate the stable layer. Cloud model studies have been suggested as a means to test some of our smallest-scale hypotheses. By determining this threshold, it would increase the confidence in issuing these warnings and predicting the type of severe weather threat possible from a storm.

REFERENCES

Bechle, A. J., D. A. Kristovich, and C. H. Wu, 2015: Meteotsunami occurrences and causes in Lake Michigan: *AGU.,* **120**, 8422-8438.

Bechle, A. J., C. H. Wu D. A. Kristovich,, E.J. Anderson, D.J. Schwab, and A.B. Rabinovich, 2016: Meteotsunamis in the Laurentian Great Lakes: *Sci Rep.*, **6**, 1-8.

Benjamin, S. G., G. A. Grell, J. M. Brown, and T. G. Smirnova, and Coauthors, 2016: A North American hourly assimilation and model forecast cycle: The Rapid Refresh. *Mon. Wea. Rev.*, **144**, 1669-1694.

Bosart, L. R., and A. Seimon, 1988: A case study of an unusually intense atmospheric gravity wave. *Mon. Wea. Rev.*, **116**, 1857-1886.

Colman, B. R., 1990a: Thunderstorms above frontal surfaces in environments without positive CAPE: Part I: A climatology. *Mon. Wea. Rev.*, **118**, 1103-1121.

Colman, B. R., 1990b: Thunderstorms above frontal surfaces in environments without positive CAPE. Part II: Organization and instability mechanism. *Mon. Wea. Rev.*, **118**, 1123-1144.

Corfidi, S. F., S. J. Corfidi, and D. M. Schultz, 2008: Elevated convection and castellanus: Ambiguities, significance, and questions. *Wea. Forecasting*, **23**, 1280-1303.

Doswell, C. A., and E. N. Rasmussen, 1994: The effect of neglecting the virtual temperature correction on CAPE calculations. *Wea. Forecasting,* **9**, 625-629.

Gilmore, M. S., and L. J. Wicker, 1998: The influence of midtropospheric dryness on supercell morphology and evolution. *Mon. Wea. Rev.*, **126**, 943-958.

Grant, B. N., 1995: Elevated cold-sector severe thunderstorms: A preliminary study. *Natl. Wea. Dig.*, **19**(4), 25-31.

Grempler, K. R., 2018: *Analysis of severe elevated thunderstorms using DCIN and DCAPE*. M.S. Thesis, School of Natural Resources, University of Missouri, Columbia, Columbia, Missouri, 91 pp.

Horgan, K. L., D. M. Schultz, J. E. Hales, S. F. Corfidi, and R. H. Johns, 2007: A five-year climatology of elevated severe convective storms in the United States east of the Rocky Mountains. *Wea. Forecasting*, **22**, 1031-1044.

Johns, R. H., and C. A. Doswell III, 1992: Severe local storm forecasting. *Wea. Forecasting,* **7**, 588-612.

Kastman, J. S., L. D. McCoy, P. S. Market, and N. I. Fox, 2017: An example of synergistic coupling of upper- and lower-level jets associated with flash flooding. *Meteorol. Appl.,* **24**, 206-210.

Market, P. S., S. M. Rochette, J. Shewchuk, R. Difani, J. S. Kastman, C. B. Henson, and N. I. Fox, 2017: Evaluating elevated convection with the downdraft convection inhibition. *Atmos. Sci. Lett.,* **18**, 76-81.

Market, P. S., K. Grempler, P. Sumrall, and C. Henson, 2019: Analysis of severe elevated thunderstorms over frontal surfaces using DCIN and DCAPE. *Atmosphere.*, **10**, 1-13.

Moore, J. T., A. C. Czarnetzki, and P. S. Market, 1998: Heavy precipitation associated with elevated thunderstorms formed in a convectively unstable layer aloft. *Meteorol. Appl.*, **5**, 373-384.

Rochette, S. M., and J. T. Moore, 1996: Initiation of an elevated mesoscale convective system associated with heavy rainfall. *Wea. Forecasting*, **11**, 443-457.

Rochette, S. M., J. T. Moore, and P. S. Market, 1999: The important of parcel choice in elevated CAPE computations. *Natl. Wea. Dig.,* **23**(4), 20-32.

Schneider, R. S. 1990: Large-amplitude mesoscale wave disturbances within the intense Midwest extratropical cyclone of 15 December 1987. *Wea. Forecasting*, **5**, 533-557.